Scientific Research Publishing

Atmospheric and Climate Sciences, 2023, 13, 103-137
https://www.scirp.org/journal/acs
ISSN Online: 2160-0422
ISSN Print: 2160-0414

Seasonal Prediction of Tropical Cyclones and Storms over the Southwestern Indian Ocean Region Using the Generalized Linear Models

Kombo Hamad Kai[1], Yohanna Wilson Shaghude[1], Christian Bs Uiso[2], Agnes Laurent Kijazi[2], Sarah Osima[2], Sara Abdalla Khamis[3], Asya Omar Hamad[1]

[1]Tanzania Meteorological Authority (TMA) and Institute of Marine Sciences (IMS), University of Dar es Salaam (UDSM), Zanzibar, Tanzania
[2]Department of Physics, University of Dar es Salaam (UDSM), TMA, Zanzibar, Tanzania
[3]Department of Natural Sciences, State University of Zanzibar, Zanzibar, Tanzania
Email: kombokai68@gmail.com, shaghude@ims.udsm.ac.tz, agnes.kijazi@meteo.go.tz, sarahosima@gmail.com, asyooo@yahoo.com

How to cite this paper: Kai, K.H., Shaghude, Y.W., Uiso, C.B., Kijazi, A.L., Osima, S., Khamis, S.A. and Hamad, A.O. (2023) Seasonal Prediction of Tropical Cyclones and Storms over the Southwestern Indian Ocean Region Using the Generalized Linear Models. *Atmospheric and Climate Sciences*, **13**, 103-137.
https://doi.org/10.4236/acs.2023.132008

Received: July 18, 2022
Accepted: March 10, 2023
Published: March 13, 2023

Abstract

Tropical cyclones (TCs) and storms (TSs) are among the devastating events in the world and southwestern Indian Ocean (SWIO) in particular. The seasonal forecasting TCs and TSs for December to March (DJFM) and November to May (NM) over SWIO were conducted. Dynamic parameters including vertical wind shear, mean zonal steering wind and vorticity at 850 mb were derived from NOAA (NCEP-NCAR) reanalysis 1 wind fields. Thermodynamic parameters including monthly and daily mean Sea Surface Temperature (SST), Outgoing Longwave Radiation (OLR) and equatorial Standard Oscillation Index (SOI) were used. Three types of Poison regression models (*i.e.* dynamic, thermodynamic and combined models) were developed and validated using the Leave One Out Cross Validation (LOOCV). Moreover, 2 × 2 square matrix contingency tables for model verification were used. The results revealed that, the observed and cross validated DJFM and NM TCs and TSs strongly correlated with each other ($p \leq 0.02$) for all model types, with correlations (r) ranging from 0.62 - 0.86 for TCs and 0.52 - 0.87 for TSs, indicating great association between these variables. Assessment of the model skill for all model types of DJFM and NM TCs and TSs frequency revealed high skill scores ranging from 38% - 70% for TCs and 26% - 72% for TSs frequency, respectively. Moreover, results indicated that the dynamic and combined models had higher skill scores than the thermodynamic models. The DJFM and NM selected predictors explained the TCs and TSs variability by the range of 0.45 - 0.65 and 0.37 - 0.66, respectively. However, verification

analysis revealed that all models were adequate for predicting the seasonal TCs and TSs, with high bias values ranging from 0.85 - 0.94. Conclusively, the study calls for more studies in TCs and TSs frequency and strengths for enhancing the performance of the March to May (MAM) and December to October (OND) seasonal rainfalls in the East African (EA) and Tanzania in particular.

Keywords

Tropical Cyclones and Storms Frequency, Thermodynamic and Dynamic Models, Skill Scores TCs/TSs Variability and Verification, Leave One out Cross Validation

1. Introduction

The short rainy season of December to March (DJFM) over the East African (EA) coast, including Tanzania is characterized by the presence of the northeast monsoon winds which induce the annual fluctuation of weather systems and hence results into the existence of favorable conditions for TSs and TCs occurrences. The meteorological and oceanographic parameters which trigger the TCs/TCs formation and their development in the SWIO basin include advected moist air from Congo air mass, long track air flows from the northeastern Indian Ocean (IO) and the northwesterly IO [1]. Other parameters include the IO monsoon trough and surges which enhances low level cyclonic circulation *i.e.* vorticity [2] [3], warmth of the ocean in areas bounded by 2.5˚ - 24˚S and 39.5˚ - 71˚E especially over the northeastern Madagascar during November to May (NM) [4] vertical wind shear at 200 - 850 mb [5] [6] [7] and mean zonal steering winds (500 - 700 mb) [8] [9] at the genesis positions of the TCs/TCs. Moreover, the fluctuations of the convection levels which move in line with the Inter Tropical Convergence Zone (ITCZ) and tele-connections such as easterly waves [3], Quasi Biennial Oscillations [1] and Madden Julian oscillations [10] are among the parameters which are considered to be responsible for the TCs/TSs genesis and development. Most of the TCs/TSs occurring in the SWIO basin is not as strong as those reported for the Atlantic Ocean basin, although there are few exceptions such as Bondo, Bongani, Gafilo, Fantala, Eline and Idai TC/TS events which were relatively strong. These TCs were accompanied with violent winds heavy rainfall and severe floods which devastated most of the Eastern African countries including Mozambique, Madagascar, Zimbabwe, Malawi and some parts of EA countries like Tanzania and Kenya [10] [11] [12] [13] [14]. Over the SWIO basin TCs/TSs landfalls (*i.e.* TCs/TSs to hit on land) frequently happens in Madagascar and rarely in Mozambique. As for the EA coast only a few occasions of TSs landfall have been reported to cross direct over EA coast with adverse impacts, these include TC Lindi, 1953 and TS Lily 1967 [15] [16] [17]. The frequency of the TCs over SWIO has been much linked with the aforementioned

environmental global large scale parameters whose monthly to seasonal fluctuation is caused by various atmospheric and oceanic oscillatory phenomena including Madden Julian Oscillations (MJO) [18] [19], Quasi Biennial Oscillations (QBO) as well as El Niño Southern Oscillations (ENSO), and the two (ENSO and MJO) normally linked to bring the changes in SSTs, tropical convection, and large-scale atmospheric circulation over vast tropical oceans on inter-annual and sub seasonal time scales [19] [20].

Different studies on the TCs characteristics and variability over the basin have been conducted both at a local level [1] [3] and over the entire SWIO basin. References [4] [20] worked on climate and weather variability over SWIO, while [2] looked at the climatologically associations and characteristics of SWIO TCs; while [3] worked on statistical prediction of TCs days. Reference [3] observed positive correlation between SST with TC frequency (TC days) over the entire SWIO during the season spanning from September to March. Moreover, their linear statistical model for forecasting TC days revealed a model fit (r^2) of 59% with a (Jackknife) cross validation resulting a correlation of 0.7 and a true model skill of 46% indicating that, their model performance was adequate. Using T42 model for the period of 1979-88, [21] showed that TCs inter-annual frequency of the ensemble mean was strongly anti-correlated with observations over the SIO, indicating that TCs frequency inter-annual variability is not consistent with observations. On further analyzing characteristics of SWIO TCs, reference [10] noted that South Indian Ocean (SIO) TCs had tracks which was more or less zonal during La Niña event and tend to be more frequent when local SSTs were relatively warm. Moreover, using Gaussian atmospheric model (TL159) and SSTs as an ENSO indicator, [10] showed the influence of La Niña conditions and warmer local SSTs on the frequency of TCs landfalls over Mozambique.

Reference [22], discussed the inter-annual variability and statistical prediction of intense TCs days whereas [23] discussed the TCs spiral rains bands, evaluation of reanalysis data using the satellite microwave (e.g. QuikSCAT and TRMM) as well as evaluating the impacts of storm surges and swells in the SWIO. Most of the statistical studies by [2] focused on prediction of TCs days over SWIO using various techniques. Though these studies provide very useful information on the understanding of TC activity and their characteristics in SWIO, but the statistical prediction of seasonal TCs counts/frequency has been given less attention over the SWIO.

In view of the above, the present study was aimed at predicting TCs and TSs seasonal counts (frequency) over the SWIO basin defined by 39.5˚E - 71˚E, 2.5˚S - 22.5˚S. Since TCs and TSs occurring over the SWIO basin, become very destructive to Tanzania and other EA countries, especially when they track over the northern Mozambique Channel [12], their impacts over Tanzania and other adjacent countries have implications on a wide range of socio-economic sectors [12] [13] [14]. Thus, baseline information on TCs/TSs frequency over the SWIO basin is needed to assist the policy makers and planners to formulate contingen-

cy plans and disaster risk reduction programmes for the TC/TS hotspots areas. Moreover, enhancement and validation of the seasonal rainfall forecasts (MAM and OND) critically needs more information/inputs about the TCs and TSs activities over the basin.

2. Methods

2.1. Study Area, Data Acquisition and Processing

The Southwestern Indian Ocean (SWIO) basin is bounded by 0˚ - 40˚S and 39˚ - 90˚E. As far as this study is concerned, the study domain was designed to be northwestern part of the SWIO defined by 2.5˚ - 22.5˚S and 39.5˚ - 71˚E as shown in Figure 1. This area was selected based on the fact that most of the TCs/TSs tracks are observed over this domain; moreover, the study was more interested on TCs which in most times affects the coastal and hinterlands of Tanzania.

The TCs/TSs datasets used in this study was acquired from International Best Track Archive for Climate Stewardship (IBTrACS) sited by (https://www.ncei.noaa.gov/products/international-best-track-archive). The data included the observations on number of TCs observed during DJFM and NM for 34 TC seasons spanning from 1977/78 to 2010/2011. Furthermore, the data contained information such as TC/TS name, date, position (in latitude and longitude), minimum surface pressure, and maximum wind speed of TCs for every 6-hours interval. Other datasets used are the large scale environmental parameters which include SST, OLR, zonal winds (u) and meridional winds (v) for different pressure levels, the datasets were acquired from NOAA NCEP-NCAR

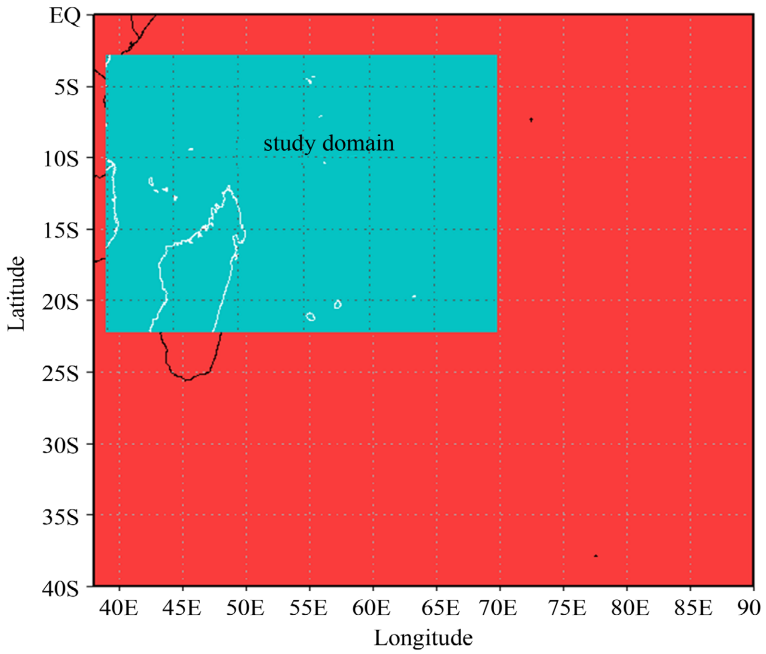

Figure 1. The SWIO basin (red); and the study domain (blue); (Source a map drawn from grads software).

Reanalysis 1 data. The data on the equatorial Southern Oscillation Index (ESOI) which covers the area over the eastern equatorial Pacific (80˚W - 130˚W, 5˚N - 5˚S) and Indonesia (90˚E - 140˚E, 5˚N - 5˚S) was obtained from the NOAA Climate Prediction Center (CPC) climate indices, while the data on Quasi Biennial Oscillations at 50 mb and 30 mb zonal wind indices, was cited by http://www.cpc.ncep.noaa.gov/data/indices/qbo.u30.index. The data on Nino 3.4 [24] defined over the region bounded by 120˚W - 170˚W and 5˚S - 5˚N was obtained from NOAA CPC. Moreover, the standard SOI was obtained from NOAA Climate Prediction Center (CPC) climate data indices and the link is (https://www.cpc.ncep.noaa.gov/data/indices/soi).

The SWIO data on TCs and TSs December to March (DJFM) seasons spanning from 1977/78 to 2010/11 was sorted to obtain TSs/TCs records that only fall in the study domain. During sorting, the data with no records of both central wind and central pressure were discarded, with most such gaps found from 1978 - 1982. Wind pressure relationship derived by [25] was used to filler the TCs/TSs records with gaps in either wind or central pressure. The Beaufort scale wind classifier was used to remove Tropical Depression (TD) records (*i.e.* 8.75 $m{\cdot}s^{-1} \leq Ws \leq 16.98\ m{\cdot}s^{-1}$), where Ws refers to wind strength/speed (https://education.nationalgeographic.org/resource/beaufort-scale). The TSs records characterized by $17.5\ m{\cdot}s^{-1} \leq Ws \leq 32.4\ m{\cdot}s^{-1}$ and TCs records characterized by $Ws \geq 32.9\ m{\cdot}s^{-1}$ were retained (https://education.nationalgeographic.org/resource/beaufort-scale).

The large scale environmental parameters including low level relative vorticity (hereafter $LLRV_{850}$) mean vertical wind shear derived from 200 - 850 mb (hereafter E_{vws}) and zonal mean steering wind speeds from 500 - 700 mb (hereafter U_{mst}) were derived from the monthly mean gridded field reanalysis products of zonal (u) and meridional (v) winds component [26]. Both u and v had spatial resolution of 2.5˚ × 2.5˚ and temporal scale spanning from April 1974 to date. The monthly gridded interpolated OLR [27] had a spatial resolution of 2.5˚ × 2.5˚. The Extended Reconstructed SST (ERSST) version 3b (v3b) [28] had a spatial resolution of 2˚ × 2˚ and spanned from 1854 to date. To customize the data and the study area, all the gridded monthly data sets were configured to fit the study domain with temporal coverage of the data, and also being configured to fit the climatological records of TSs and TCs datasets which spanned from 1978-2011 (with the exception of OLR which spanned from 1979 to 2011 *i.e.* 1978 did not have enough data records for this variable). After this configuration, the long-term monthly and seasonal averages were calculated.

Environmental vertical wind shear (E_{vws}) which is defined as the magnitude of the vector difference of winds between 200 and 850 mb pressure levels [29] [30] given by:

$$E_{vws} = \sqrt{\left(U_{200} - U_{850}\right)^2 + \left(V_{200} - V_{850}\right)^2} \quad (1)$$

where U_{200} and U_{850} represent the zonal winds at 200 - 850 mb and V_{200} and V_{850} represent the meridonal winds at 200 - 850 mb, respectively.

E_{vws} is a crucial component for the development and weakening of TCs [31] [30] and it is inversely related to vertical uplifting of moisture in the TCs environment [32]. $LLRV_{850}$ was computed using a centered finite-differencing scheme, and U_{mst} was obtained by averaging the zonal winds (u) wind at 500 and 700 mb. This data was used based on the fact that mid tropospheric flow associated with 500 - 700 hPa gives the best correlations with cyclone movements [33].

Furthermore, the global and regional indices of ENSO, Nino 3.4 indices, ESOI and 30 - 50 mb QBO was calculated into monthly and seasonal averages of September to November (SON) and June to August (JJA), as well as the running mean for DJF season. Moreover, the QBO absolute difference *i.e.* |50 - 30| for each month and each season were also determined

2.2. Inter Annual Variability and Correlation between TCs and Gridded Parameters

In this study, five gridded parameters were used in searching for the potential predictors; these include SST, OLR, $LLRV_{850}$, E_{vws} and U_{mst}. After being processed into seasonal and monthly averages, the point to field correlations maps between TCs and TSs frequency and these gridded parameters within the domain defined by 70˚W - 120˚E and 45˚S - 45˚N at $p \leq 0.05$ were determined (for example contours in **Figure 4**). The monthly time leads of November backwards to June (6 months leads) and seasonal leads of September to November (SON) and June to August (JJA) were used for developing these correlations. Areas with high correlations (of $r \geq \pm 0.35$) were identified and extracted using Grid Analysis and Display System (GrADS) software. Moreover, inter annual variability of the extracted area averages values of gridded parameters and season TCs and TSs frequency were analyzed to deduce the major patterns of the variability. Apart from the correlation between the global and regional indices, the inter-annual variability of TCs and TSs with ESOI, QBO, ENSO and Nino 3.4 indices were plotted and analyzed.

2.3. Identifying and Selecting Potential Predictors and Modeling Procedures

In determining the potential predictors to be used in forecasting model the following criterions were used: 1) the sign of correlation between the predictor and TSs/TCs frequency. This was used based on the nature of the relationship between the predictor and TSs/TCs. In this process the predictors with low correlations with TCs or with correlation which opposes the relationship between the TCs and that particular predictor were filtered out; 2) the strength of the correlation and inter-annual variability plots for TCs/TSs frequency and that of predictor were used to determine how the phases and trends of the two curves (TCs/TSs frequency and the predictor) were matched. 3) Other criterion used includes a) persistence of the predictor before the onset of TS/TC season, b) the correlation between the observed and the cross validated (forecasted) TCs/TSs

(*i.e.* how good the phase was captured by the model), and c) the significance of the chi (χ^2) squared test between the model residual and deviance (*i.e.* model goodness of fit). The generalized linear models (GML) with the Poisson family (*i.e.* Poisson model) were used. The model was used to determine whether there was a strong relationship between each type of potential predictors (single parameter models) and predictands. Apart from single parameter models, multi-parameters models including the thermodynamic, dynamic and the combined models (*i.e.* combination of dynamic and thermodynamic parameters) were also developed.

The log linear Poison regression model was used to predict the DJFM and NM TSs and TCs. The choice of this model in preference to the linear statistical models (e.g. least square models) was based on its improved hindcast skill [34]. The model is often used to forecast the occurrence of rare and discrete events, such as tornado counts, droughts occurrences, or cold spells, and even earthquakes [35] [36] [37]. Moreover, the Poisson distribution restricts the possibility of having negative outcomes making it an ideal tool for forecasting TCs occurrences [29] [36]. With this model, the probability distribution *i.e.* probability of occurrence of exactly y TCs, is given by the equation:

$$Y_i \sim \text{Poisson}\left(\lambda_i\right) \tag{2}$$

where, $\lambda_i = \exp\beta_0 + \sum_j \beta_j X_{ij}$. The above equation can be expressed by a log linear equation given by:

$$\ln\left(\lambda\right) = \beta_0 + X'\beta \tag{3}$$

where

$$X_i \in \left\{\text{SST}_i + \text{VORT}_i + \text{OLR}_i + \text{EVWS}_i + \text{UMST}_i + \text{NINO3.4}_i + \text{SOI}_i + \text{QBO}_i\right\}$$

$$i = 1, 2, 3, \cdots, N$$

$$\beta_j \in \left\{\beta_0, \beta_{\text{SST}}, \beta_{\text{VORT}}, \beta_{\text{OLR}}, \beta_{\text{EVWS}}, \beta_{\text{UMST}}, \beta_{\text{NINO3.4}}, \beta_{\text{SOI}}, \beta_{\text{QBO}}\right\}$$

In the above equations, the potential predictors $X_{(i)}$ could be SST, LLRV_{850}, OLR, E_{VWS}, U_{MST} or Nino 3.4 indices, where β_0 stands for model intercept, and β_1 to β_n are the model coefficients based on the number of predictors.

Though TCs are developed from TSs (*i.e.* TCs depends on further intensification of TSs), but their prediction was undertaken independently. This is because both TSs and TCs have impacts to the western SWIO countries; moreover, it is not necessary for each tropical storm to develop into matured TC. In the thermodynamic model, the environmental variables of SST, OLR and SOI/ESOI were used as potential predictors, whereas in the dynamic model the environmental variables of U_{mst}, E_{vws} and LLRV_{850} were used as potential predictors where in the combined model both dynamic and thermodynamic potential predictors were used.

2.4. Leave One Out Cross Validation and Verification Technique

Many seasonal TCs forecasting studies including [29] [33] [36] [38] among oth-

ers, have used the Leave One Out Cross Validation (LOOCV) techniques to assess the skill of their models for unseen data. This study used the LOOCV technique [34], where one case was left out as the testing case and the remaining cases were used to build the model. The same procedure was repeated for all data cases (*i.e.* entire length of the predictors), where the output of this prediction was referred to as a hindcast if the predicted outcome was known and forecast if the predicted outcome was not known. Evaluation of the model performance for future use is considered to be a very important aspect in modeling discipline [34] [39]. This can be achieved by: 1) correlation analysis between the hindcast/forecast and the observations 2) determining the root mean square error (RMSE) or mean absolute error (MAE). In this study the RMSE and MAE were used to evaluate the performance of the models. The MSE is closely related with the average accuracy of the forecast as it maps the clustering of residuals around the regression line, where tightly clustering corresponds to low values of MSE and vice versa. For TCs prediction RMSE of the hindcast/forecast provides a measure of the model hindcast/forecast skill by comparing the amplitudes of the observed and predicted TCs. The closer the hindcasts/forecasts to the observation the lower the RMSE and the better is the model.

In this study our model skill was evaluated using both the RMSE of the hindcasts and that of the persistence (*i.e.* climatological forecasts). The RMSE for the hindcast is given by:

$$\mathrm{RMSE}_{\mathrm{h}} = \sqrt{(1/n)\sum_{i=1}^{i=n}\left(y_i - \sigma_i\right)^2} \tag{4}$$

where y_i is the i^{th} observation and σ_i is the i^{th} hindcast and n is the length of both observations and hindcast.

Where the RMSE for the persistence or climatology is given by:

$$\mathrm{RMSE}_{\mathrm{clim}} = \sqrt{(1/n)\sum_{i=1}^{i=n}\left(y_{i\mathrm{clim}} - \sigma_i\right)^2} \tag{5}$$

where $y_{i\mathrm{clim}}$ is the number of TCs predicted using only months, latitude and longitude as predictors, this will be the same number predicted each year.

Hence based on [40] the skill score (SS) of the hindcast was obtained using Equations (4) and (5) calculated as follows

$$\mathrm{ss} = 1 - \left(\mathrm{RMSE}_{\mathrm{p}} / \mathrm{RMSE}_{\mathrm{clim}}\right) \tag{6}$$

where the $\mathrm{RMSE}_{\mathrm{p}}$ indicates the root mean square error of the predicted model, and the values for the SS lies between 0 and 1; When SS = 1 indicates a perfect model hindcast; SS = 0 indicates hindcast that are only accurate as the reference climatology; SS ≤ 0 indicates the forecast that are less accurate than the reference.

After cross validating the models, we constructed the two ways contingency tables for model verification. We used the R software to construct the 2 × 2 square matrix using the forecasts and observations of DJFM and NM TSs and

TCs frequency. This square matrix was based on hit rates which showed whether the event was forecasted (F)/not forecasted (NF) and being observed (OB)/not observed (NOB). Moreover, we performed the analysis of contingency tables based on, 1) Percent correct (pc); 2) Bias of the model (which measures the correspondence between average forecasted and observed); 3) Critical success index (CSI) and 4) the false alarm ratio. We used forecast verification for assessing the quality of our forecasts, as well strengths and weaknesses of our forecasts.

3. Results

3.1. Inter Annual Variability of TCs and TSs

The results of the inter annual variability of TCs and TSs frequency for the DJFM and NM seasons presented in Figure 2 show that, the TCs frequency during the DJFM (Figure 2(a)) and NM seasons (Figure 2(b)) were characterized

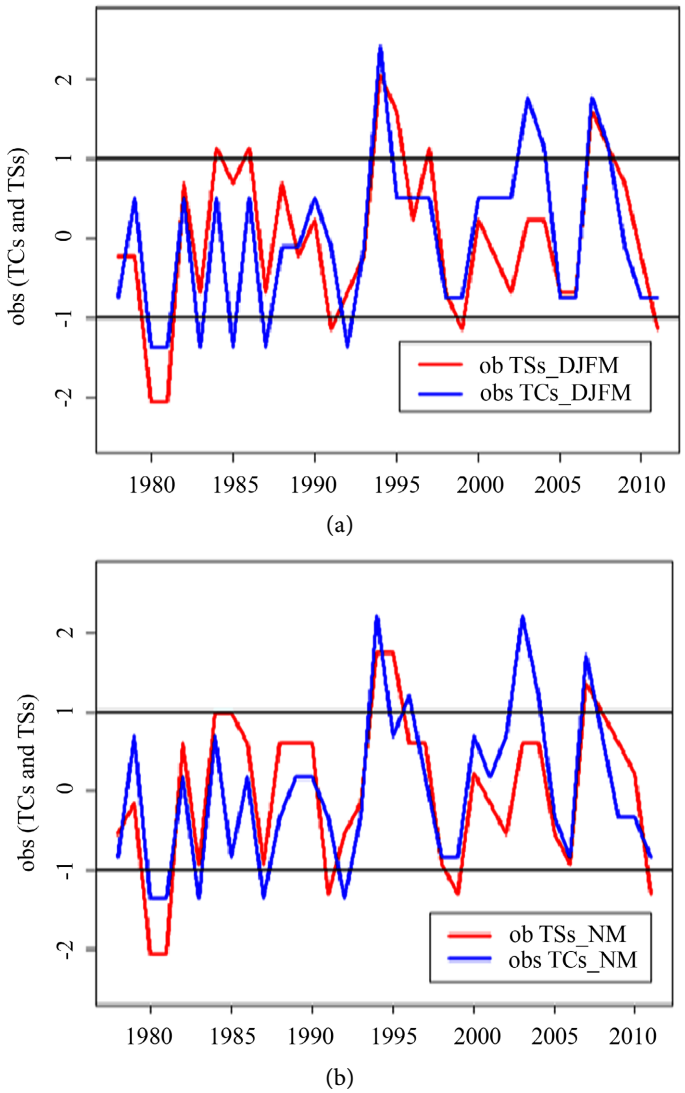

Figure 2. Inter annual variability of observed DJFM TCs and TS showing the years where their frequency is $\sigma \geq -1$ and $\sigma \geq 1$ where σ is the standard deviation of TCs frequency.

by high inter-annual variability but with higher frequency after 1994 than before 1994. The periods marked by 1994, 2003 and 2007 were marked by higher TCs/TSs frequency for both seasons. Moreover, results of inter annual variability of DJFM TCs and TSs presented in **Figure 2(a)** show that, the periods during which the TC/TS frequency exceeds one standard deviation (*i.e.* TCs/TSs frequency are $\leq -1\sigma$ or $\geq 1\sigma$) coincides with the either El Nino or La Nina events. For instance, during 1980 some TCs and TSs frequency were less than -1σ, 1985 TS frequency was greater than 1σ, 1991-1992 both TCs and TSs frequency was less than -1σ), 1994-1995 (where both TC and TS were greater than 1σ), 1997 (where TS was greater than 1σ), 2004 and 2007 both TCs and TSs frequency exceeded 1σ. Besides the results show that TCs frequency lower peaks which are less than -1σ (e.g. of 1983/84, 1985/86) were aligned with weak La Nina, while TCs frequency which was greater than 1σ (e.g. 1987/88) was aligned with strong El Nino events. Further results in **Figure 2** revealed that the TCs frequency during 1994/95, 2003/04 and 2004/05 were aligned with moderate El Nino events with the exception of TCs frequency of 2007/08 which was aligned with moderate La Nina events. The coincidence of TCs high/low TCs/TSs frequency with ENSO (El Nino/La Nina) conditions is well supported by the existence of strong correlations (with correlation factor, r = 0.4 and r = 0.3) between ENSO indicators (such as DJF ESOI and SON and DJF OLR standardized departures) with the observed DJFM TCs and TSs. Thus, the alignment of high TCs frequency (either less than -1σ or greater than -1σ) with La Nina/ El Nino indicates that, ENSO condition which have its high phase during DJF [20] could be among the factors which affect inter annual variability of TCs/TSs frequency in SWIO.

Furthermore, the inter-annual variability of DJFM and NM TSs and TCs frequency with ESOI for February and April presented in **Figure 3** showed that, there exists a higher level of positive association between TSs/TCs frequency with ESOI indicating an increase of TCs activities subjected to increasing ESOI. For instance, the inter annual variability of DJFM and NM TCs/TSs frequency with the ESOI for February presented in **Figure 3(a)** showed that, the TCs/TSs frequency patterns are well captured by ESOI patterns except for some few cases (e.g. from 1994 onwards both TSs and TCs have shown an increasing trend, the same feature is shown by February ESOI). Inter annual variability of DJFM and NM TCs/TSs with the April ESOI (**Figure 3(b)**) almost had the same features as that of **Figure 3(a)**.

The analysis of correlation between the DJFM and NM TCs/TSs with Ocean Nino Indices (ONI) anomalies at Niño 3.4 region revealed that Nino 3.4 indices for SON, JJA, and August to October (ASO) had significant negative correlation with DJFM TCs frequency with r values of −0.37 (p = 0.03), −0.4 (p = 0.02) and −0.32 (p = 0.06 not significant). This negative correlation may signify that, DJFM TCs frequencies are more favored by La Nina conditions rather than El Nino as agreed by [20]. This is also supported by [40] who noted that, ENSO causes a geographical shift in the positions of TC maxima. As for the correlation

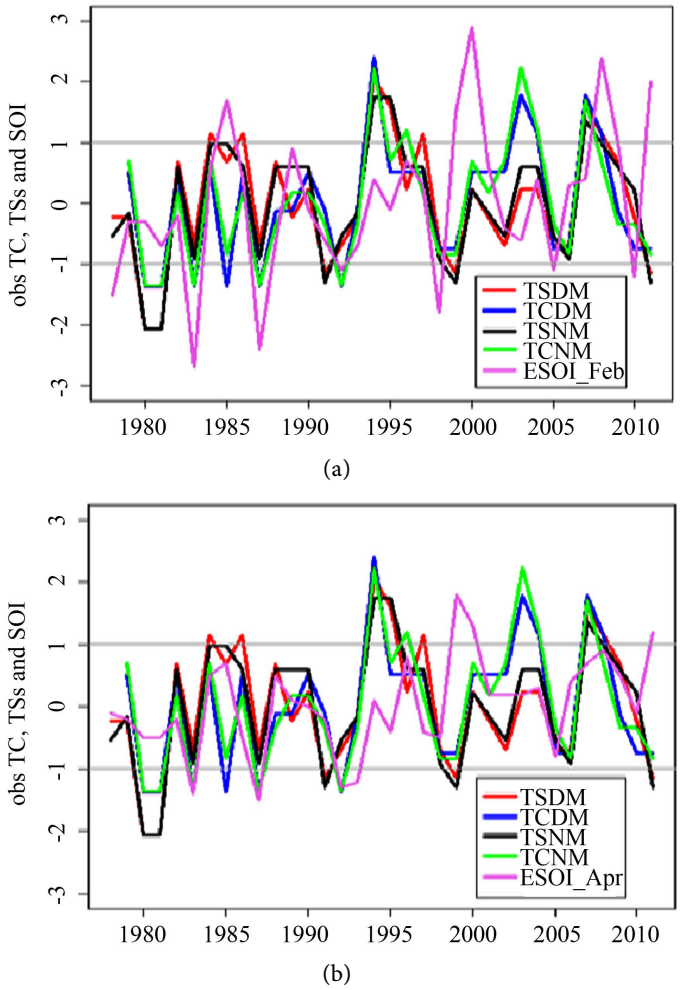

Figure 3. Inter annual variability of DJFM and NM TSs and TCs with E SOI where (a) DJFM and NM TCs and TSs with February SOI; (b) same as (a) for April SOI.

between the ESOI and DJFM and NM TSs/TCs results revealed significant correlation (r = 0.32 to 0.36), indicating that the curves for ESOI and DJFM and NM TCs/TSs are well phased (**Figure 3**).

3.2. The Influence of Sea Surface Temperatures on Tropical Cyclones and Tropical Storms

The analysis of monthly mean SST patterns as precursor of TCs over SWIO during JJA and SON (early TCs season) presented in **Figure 4** show that, over Southern Indian Ocean (SIO) from JJA (**Figure 4(a)**) to SON (**Figure 4(b)**) there exists a southward shift of higher SSTs about 6˚ - 8˚ latitude contoured by a 27˚C to 33˚C isotherm, followed by a westward shift of about 2˚ longitudes over Somali Sea. This condition could be explained by the east west fluctuation of IOD, propagation of Ocean Rossby wave activity from SIO to SWIO and also reflection of the Ocean Rossby waves. Moreover, the results in **Figure 4(b)** shows a northward shift of higher SON means SSTs over the northern Atlantic Ocean (NAO).

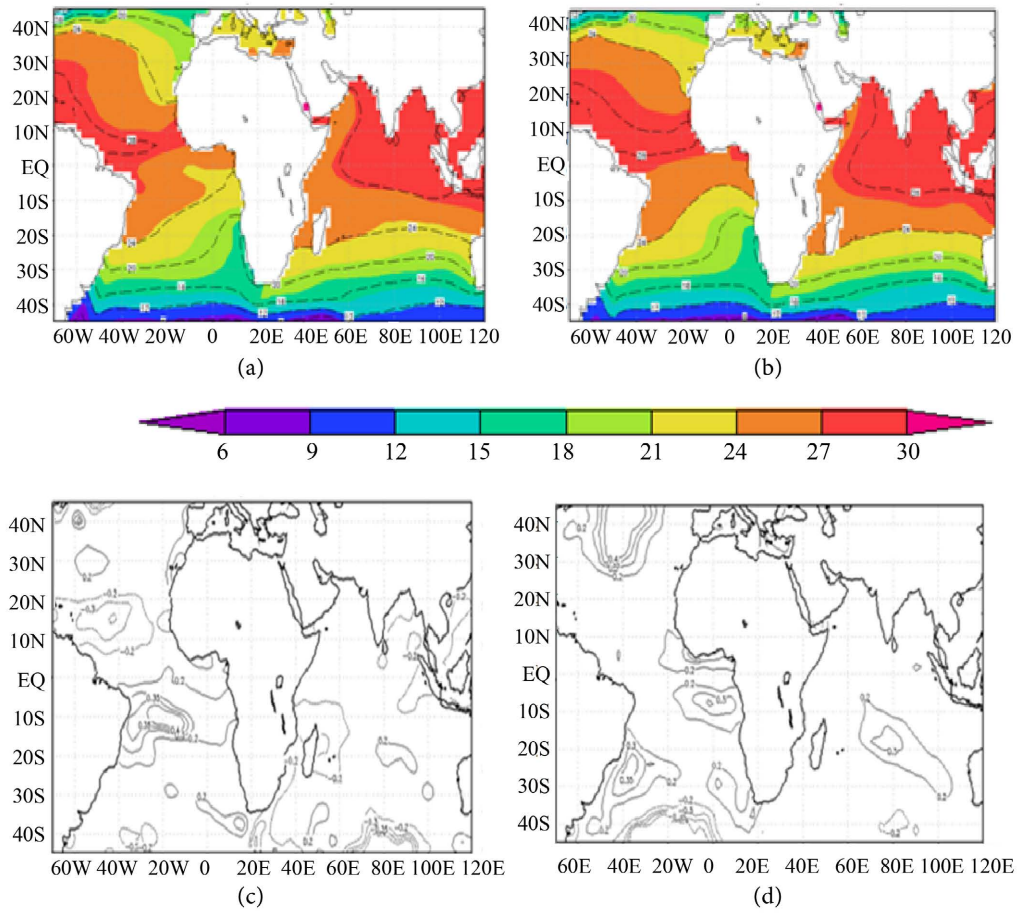

Figure 4. SST distribution over Southern Indian Ocean (SIO) during JJA (a) and SON (b). Monthly average JJA (a) and SON (b) SSTs and the correlation coefficients for the NM TCs with June SSTs (c) and NM TSs with SON SSTs (d).

The correlation analysis between TCs frequency variability with Oceanic and atmospheric predictors, revealed that SON SSTs have positive correlation with NM TCs frequency of up to 0.4 at North Atlantic Ocean at 30˚ - 48˚W and 27˚ - 45˚N and SIO at North Eastern Reunion at 63˚ - 83˚E and 10˚ - 22˚S. Over southern Atlantic Ocean both negative and positive correlations of about r = ± 0.35 were developed (**Figure 4(c)**). For JJA results revealed negative correlations of up to 0.35 with TCs in DJFM over the SIO (65˚ - 115˚E and 38˚ - 45˚S) (**Figure 4(d)**). Generally, the monthly mean SSTs revealed that September to November were having significant positive correlation at various regions of Atlantic and SIO; whereas July to August were having weak correlations, implying that, DJFM TCs have weak association with JJA gridded mean SSTs over SIO and Atlantic Ocean during JJA (**Figure 4(c)** and **Figure 4(d)**). On the other hand, correlations between NM TCs frequency with SON SSTs at $p \leq 0.05$ revealed the existence of highest positive correlations of up to 0.4 at NAO region bounded by 30˚ - 50˚W and 30˚ - 45˚N, while for September the results show a correlation of up to r = 0.35 mapped at 30˚ - 40˚W and 20˚ - 30˚S, and for June SSTs higher r values (*i.e.* $r \leq +0.35$) were concentrated around 10˚ - 30˚W and 5˚

- 15˚S at Southern Atlantic Ocean (SAO). In general point to field correlation between monthly and seasonal SSTs with DJFM and NM TCs/TSs were mainly concentrated on both Indian and Atlantic Oceans. Moreover, data from highly correlated areas (*i.e.* at r ≥ ±0.35) were extracted.

3.3. The Influence of E_{vws}, U_{mst}, and $LLRV_{850}$ to the Tropical Cyclones Frequency

The analysis of the monthly and seasonal averages of E_{vsw} for JJA, SON, DJF, and DJFM revealed a southward shift of low E_{vws} values as we approach the peak TCs season. This could be explained by the positional variation of ITCZ. The southward shift of low E_{vws} widely seen when you cross examine the position of 10 $m{\cdot}s^{-1}$ E_{vws} contour during JJA, SON and DJFM (**Figure 5**) over the tip of Madagascar and at Southern Atlantic Ocean. Moreover, results in **Figure 5** revealed a timely positioning and division of equatorial (8˚N - 12˚S) 10 $m{\cdot}s^{-1}$ E_{vws} contour over eastern, central and western closed contour as shown in **Figure 5(b)**. This timely position of low E_{vws}, contours could be associated with tropical convection bands during north-south and east-west oscillations of ITCZ. This fluctuation and oscillations of E_{vws} creates the good environments to TCs genesis and development [7] [41]. Results of the point to filed correlations between DJFM and NM TCs/TSs frequency with monthly and seasonal area averaged E_{vws} (Figures were not given) revealed that, Southern American areas (30˚ - 60˚W and 18˚ - 26˚S), northern Indian Ocean (40˚ - 60˚E and 0˚ - 10˚N) at Somali Sea, South Eastern South America (30˚ - 70˚W and 17˚ - 25˚S) and Northern Asia (40˚ - 60˚E and 40˚ - 45˚N) had highest correlations.

The results of the analysis U_{mst} (*i.e.* both seasonal and monthly) revealed that, latitude range of 10˚N - 10˚S was contoured by low U_{mst} values ranged by $-5 \leq U_{mst} \leq 0$ $m{\cdot}s^{-1}$ (weak westerly winds) (**Figure 6(a)**). These low U_{mst} values (weak westerlies) are contoured from north to south e.g. during June highest contour over the stated region was -10 $m{\cdot}s^{-1}$, with a zero contour at the tip of Mozambican channel whereas in November highest contour was -5 $m{\cdot}s^{-1}$ with zero contour retreated just southern tip of Madagascar (**Figure 6(b)**). The long term DJFM U_{mst} over SWIO could lies between -5 $m{\cdot}s^{-1} \leq U_{mst}$ 0 where towards more negative U_{mst} indicate stronger TCs and vice versa. The results of the correlation between U_{mst} and DJFM and NM TCs/TSs had shown similar results to that of E_{vws}, and areas bounded by 0˚ - 10˚N and 30˚ - 70˚W to 60˚ - 80˚E, were mapped with higher correlations. Moreover, high correlation between U_{mst} with NM and DJFM TCs and TSs frequency was mapped over the continental areas of Northern to Southern Africa, East and West Africa and North and Southern America whereas over the Ocean, high correlations were mapped over Mediterranean Sea, Atlantic Ocean and Indian Ocean were also among the areas which results into significant high negative correlations.

The analysis of the influence of seasonal and monthly average $LLRV_{850}$ on TCs over SWIO (**Figure 7**) have mapped higher vorticity values during SON of up to -10×10^{-6} s^{-1} over areas with high DJFM TCs tracks, whereas during DJF,

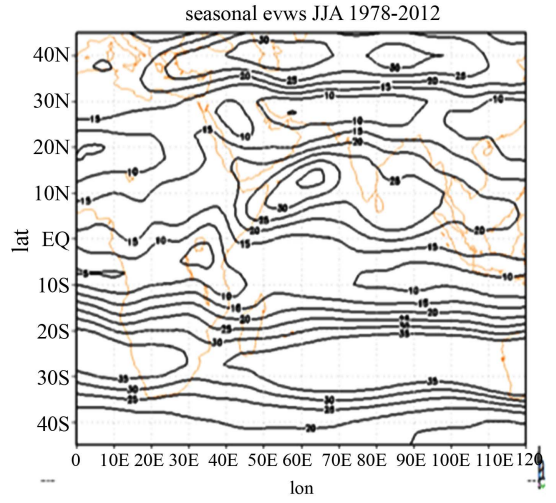

(a)

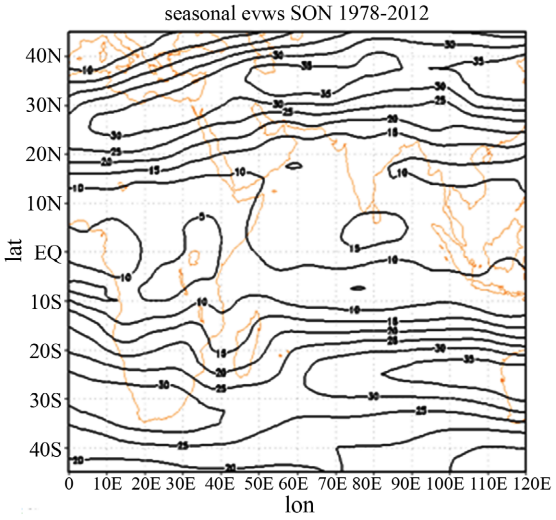

(b)

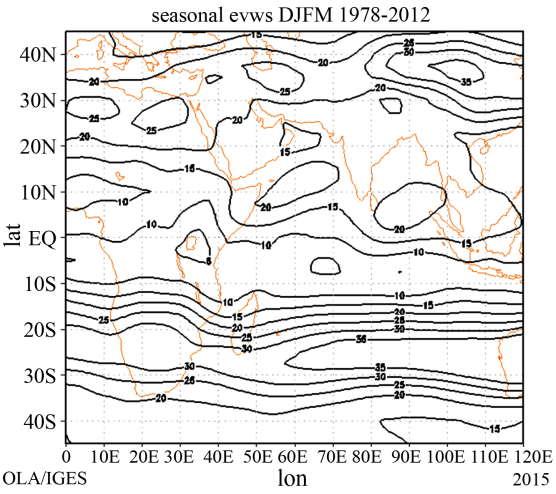

(c)

Figure 5. The long term seasonal zonal mean winds (umst) where (a) represents the JJA and (b) represents the SON and (c) represents DJFM (peak TCs season).

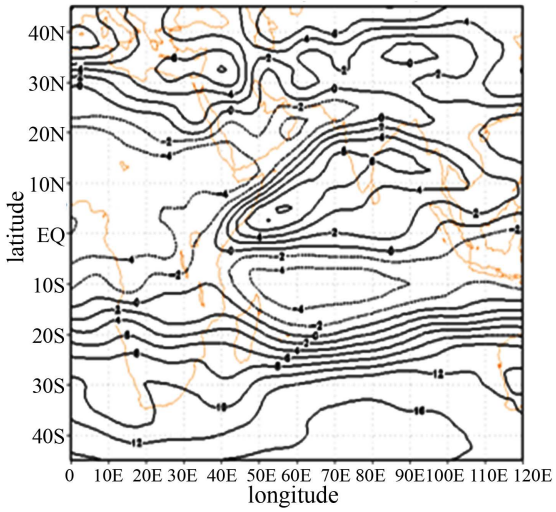

(a)

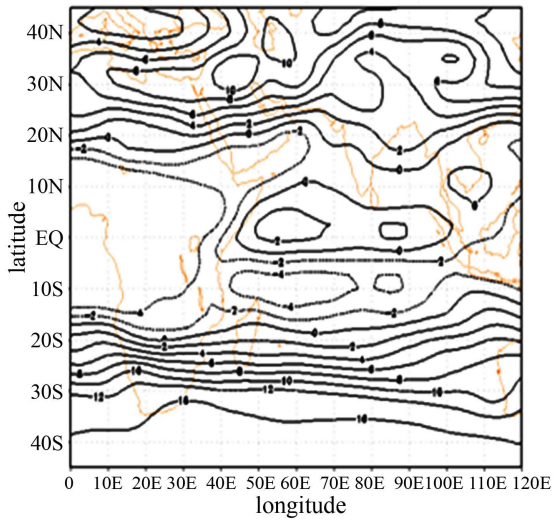

(b)

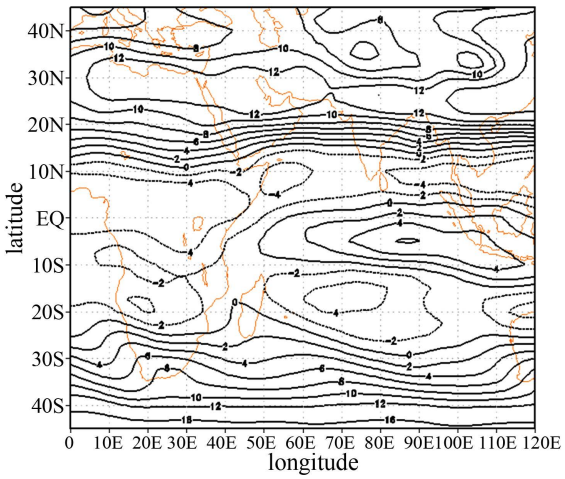

(c)

Figure 6. Seasonal mean U_{mst} (1978-2011); where (a), (b), and (c) represent JJA, SON and DJFM, respectively.

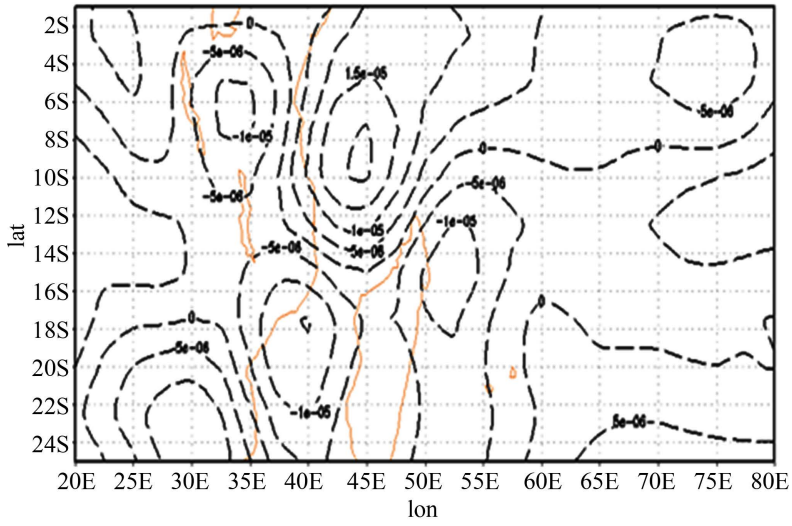

(a)

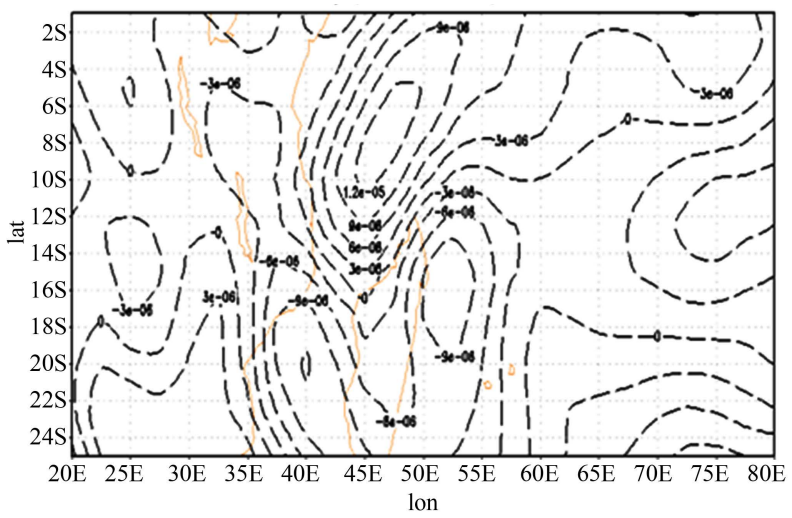

(b)

Figure 7. Variation of long term $LLRV_{850}$ (a) for SON and (b) for DJF.

$LLRV_{850}$ contours of -3×10^{-6} s^{-1} to -9×10^{-6} s^{-1} were mapped on off eastern Madagascar. The latitude ranges of 5˚ - 10˚S were under the influence of a northeasterly trough of positive $LLRV_{850}$ indicating the influence of northeasterly monsoon winds as platforms for TCs genesis. The correlation between $LLRV_{850}$ with DJFM and NM TSs/TCs (Figures were not shown) were mapped over SWIO TCs prone regions with $r \geq \pm 0.35$. The areas having these significant high correlations occurred over both Indian and Atlantic Oceans whereas over continents high correlations were mapped over southwestern African coast, Northwestern South America, West Africa and Ethiopian highlands. The correlation of $LLRV_{850}$ with DJFM and NM TSs and TCs during June to August (JJA) period had most areas with higher negative correlations than early TCs season of SON where most correlations were marked equator ward of 20˚N - 20˚S. Negatively correlated areas were favoured because TCs frequency increases with low values

of $LLRV_{850}$ as noted by [7] [42] [43] [44].

3.4. Influence of Outgoing Longwave Radiation on Tropical Cyclones and Storms Frequency

The influence of OLR to the DJFM and NM TCs/TSs showed that, the monthly (July and November) and the seasonal (SON and DJF) had average values aligned on the Northeast (NE) to Southwest (SW) direction, with low OLR values ranged from 200 - 260 $W \cdot m^{-2}$ over SWIO TCs prone areas. Results of monthly spatial distribution of low OLR from July to November presented in **Figure 8(a)** and **Figure 8(b)** revealed that, during July (**Figure 8(a)**) lowest OLR

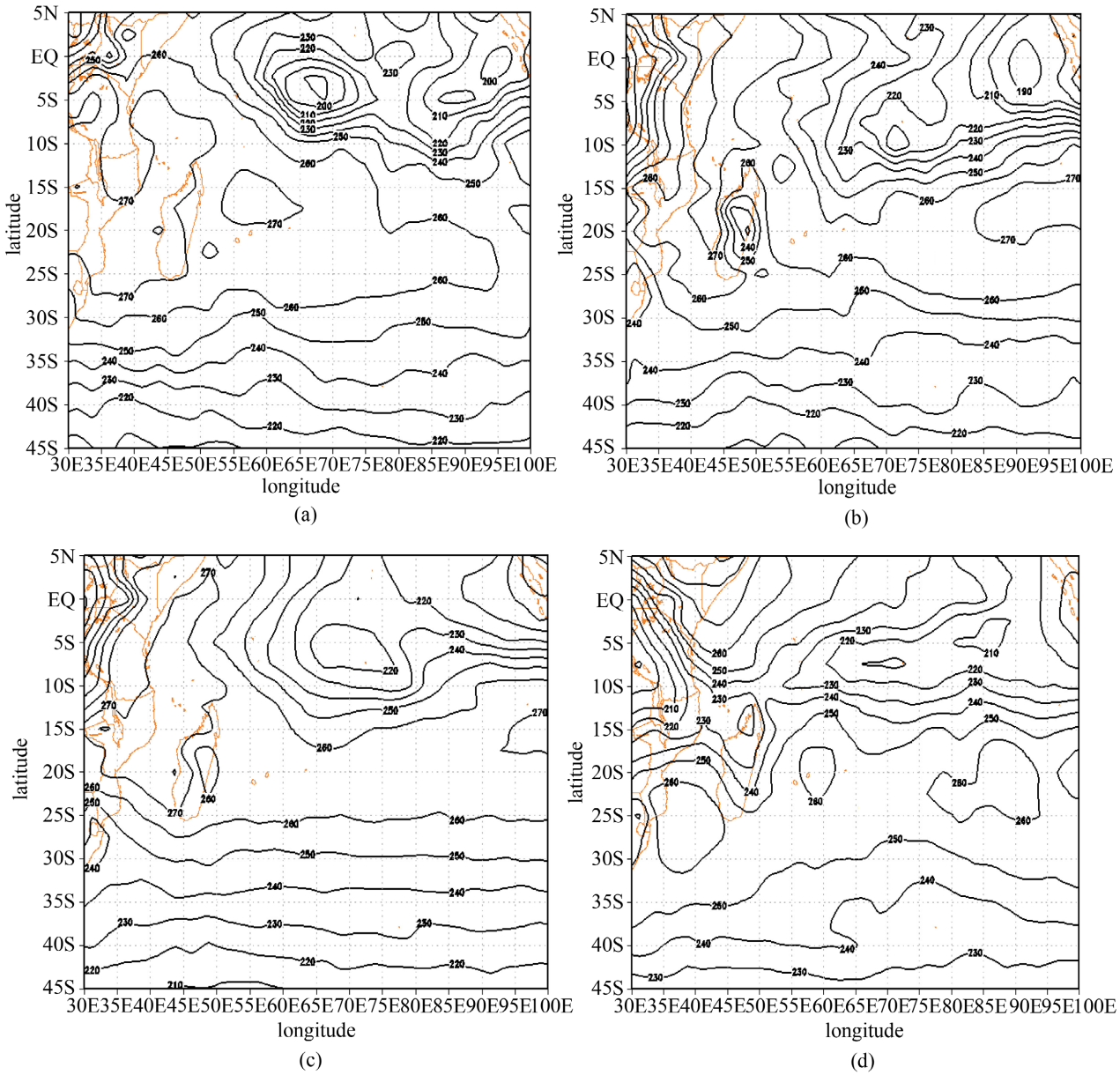

Figure 8. Monthly mean OLR spanning from 1982-2012 for July (a) and November (b) and seasonal mean for SON (c), and from 1982-2011 for DJF (d).

value of 200 W·m^{-2} was centered at 0˚ - 5˚S and 60˚ - 70˚E, whereas over the eastern Madagascar, low OLR value of 270 W·m^{-2} was centered at 15˚ - 20˚S and 50˚ - 65˚E. As for November (Figure 8(b)) lowest OLR shifted more southwest ward and centered at 5˚ - 10˚S and 70˚ - 75˚E. Moreover, the seasonal distribution of low OLR values had same alignment like monthly. For instance, during SON (Figure 8(c)) results show that, the locations of deep convection (up to 200 Wm^{-2}) were aligned few degrees south and north of the equator within grid boxes defined by 60˚ - 80˚E and 5˚N - 8˚S, 80˚ - 100˚E and 5˚N - 5˚S over the Indian Ocean; whereas over the continent the deep convection was marked over the region bounded by 5˚N - 5˚S and 20˚ - 35˚E (northwestern Tanzania and the Democratic Republic of Congo). During December to February (DJF) Figure 8(d) show that deep convection was shifted more southward with northeast alignment (values up to 200 W·m^{-2}). This shift of low OLR values, resulted into low convection band width reduction and northward penetration at (35˚ - 55˚E and 10˚S - 5˚N) of low convection band, Over the continent the high convection belt over Congo shifted southward resulting into deep convection zone covering Mozambican channel and Madagascar (Figure 8(c)) to be northwesterly shifted by Oceanic high convection resulting into compressing of both Oceanic and continental low convection belt.

The correlation (r) between OLR and DJFM and NM TSs/TCs at $p \leq 0.03$ (Figures was not shown) gave higher r values of up to −0.44, with negative correlations especially during June to August during June to August were dominated over Northern to Northeastern Madagascar and Northern (40 - 45˚N and 20 - 26˚W) and equatorial Atlantic Ocean. This JJA, SON and DJF mapping of deep OLR and their significant correlations at different Oceanic and continental areas revealed the high predictive skill of OLR to NM TCs and DJFM TCs and TSs over Southeastern Indian Ocean, Atlantic Ocean and Mediterranean Sea

3.5. Performance of Various Environmental Parameters as Potential Predictors for the Single Parameter Models for November to May Season

The performance of five environmental parameters (SST, OLR, E_{vws}, U_{mst} and $LLRV_{850}$) as the potential predictor was assessed using Poisson's regression equations, with graphical plots of the model output curves for each environmental parameter shown in Figure 9. The summaries on the performance of the five environmental parameters are shown in Table 1.

When SST was used as a potential predictor, the model output curve that was drawn to fit the observed NM TC values were given by:

$$\ln\left(\mathrm{NMTCs}_{\mathrm{sst}}\right) = -16.05 + 0.85 * a_b + 0.43 * a_c \tag{7}$$

where a_b = October SST at Southwestern AO and a_c = equatorial SOI during April.

Apart from October, other potential predictors for NM TCs which were investigated included: September North Atlantic SST, November north Atlantic

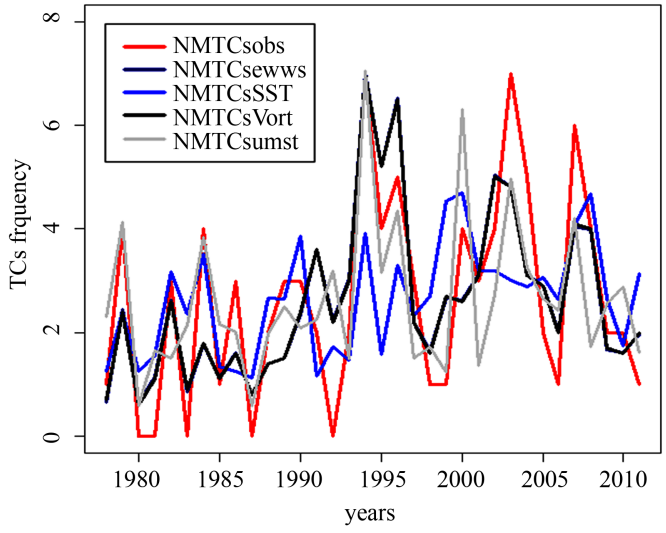

(a)

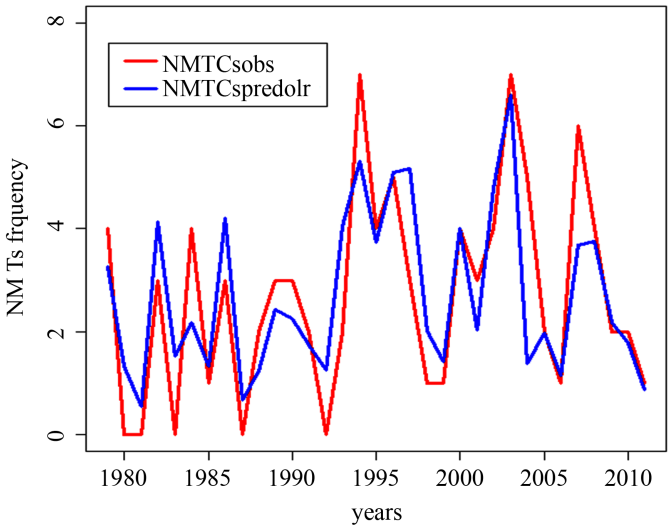

(b)

Figure 9. NM TCs model output for (a) E_{vws} (dark blue), SST (blue), Vort (black), and U_{mst} (gray); (b) OLR (blue). The red curves represent the observed NM TCs.

Table 1. Performance of environmental parameters in fitting the TCs frequency during NM season using the Poisson regression model.

Environmental parameter	Correlation (r) between observed and fitted	P value	MAE SS %	MSE SS %
SST	0.54	0.001	21	30
E_{vws}	0.76	0.01	41	57
U_{mst}	0.73	0.01	31	53
$LLRV_{850}$	0.78	0.01	35	60
OLR	0.87	0.01	43	61

Note that SS indicates the Skill Score.

SST, and October North Atlantic SST but these predictors were inferior to October SST and were therefore discarded. SSTs potential predictors over Indian Ocean were filtered using a correlation threshold of r ≥ +0.35. Analysis of the SST model performance revealed significant z scores, and χ^2 of 0.83, suggesting that the model fitted the data very satisfactorily. Moreover, correlation between observed and fitted SST TCs model during NM season gave a strong correlation (r = 0.54 at p ≤ 0.001), with the skill score of 21% and 30% based on MAE and MSE. The results of the SST TCs model **Figure 9(a)** (blue curve) indicated that April equatorial SOI and October Southwestern Atlantic Ocean SST was poor environmental parameters for predicting NM TCs.

As for E_{vws} its fitted model (**Figure 9(a)** red curve) was given by:

$$\ln\left(\mathrm{MNTCs}_{E_{vws}}\right) = 6.95 - 0.12 * d_{14} - 0.11 * e_{20} - 0.12 * d_3 \tag{8}$$

where d_{14} = September E_{vws} at Somali sea, e_{20} = November North Atlantic Ocean E_{vws} and d_3 = June southwestern Tanzania E_{vws}. The model had a significant z scores (p ≤ 0.01) with negative β values (see Equations (5) and (6)) indicative of a negative exponential relationship between E_{vws} and TCs. The correlation between the observed and the forecasted E_{vws} NM TCs was very strong (r = 0.76; p ≤ 0.01), whereas the model skills based on MAE and MSE were 41% and 57% respectively, suggesting that the E_{vws} had a better performance in predicting NM TCs compared to the SST.

The Poisson regression equation fitting the model for U_{mst} was given by;

$$\ln\left(\mathrm{NMTCs}_{\mathrm{Umst}}\right) = 2.54 - 0.12 * h_9 - 0.13 * h_5 - 0.17 * h_{13} \tag{9}$$

where h_9 = July Southeastern AO, h_5 = July North Africa, and h_{13} = August Southeastern Asia **Figure 9(a)** (gray curve). The model had a significant z score (p ≤ 0.01), with a higher degree of goodness of fit (χ^2), and negative β coefficients. The model gave a strong correlation between observation and the fitted U_{mst} TCs (r = 0.73 at p ≤ 0.01) suggestive of a strong relationship between U_{mst} and NM TCs. Like E_{vws}, the observed model skill based on MAE and MSE were 31% and 57% (**Table 1**), respectively.

The filtering process of the $LLRV_{850}$ predictors in fitting NM TCs retained Uv_{13} = October Southern Madagascar, Uv_{19} = November Eastern Namibia, Uv_{24} = September North Eastern Madagascar and Uv_{26} = September Eastern Namibia as the best potential predictor. The output Poisson's regression equation for fitting the data was given by

$$\begin{aligned}\ln\left(\mathrm{NMTCs}_{\mathrm{vort}}\right) = {} & 1.12 - 0.39\times10^5 * Uv_{19} - 1.95\times10^5 * Uv_{26} \\ & - 1.23\times10^5 * Uv_{24} - 6.12\times10^4 * Uv_{13}\end{aligned} \tag{10}$$

The output curve for vorticity model is presented in **Figure 9(a)** (black curve). The model presented in Equation (5.6) had a significant z scores (p ≤ 0.01) for most potential predictors, with Uv_{13} increasing the model goodness of fit and the skill by 20. The $LLRV_{850}$ model **Figure 9(a)** (black curve) showed a strong correlation (r = 0.78; p ≤ 0.01) between the observed and fitted NM TCs, with the ob-

served and fitted being almost in phase. The model skills based on MAE and MSE skill scores were estimated at 35% and 60%, respectively suggesting that the $LLRV_{850}$ had highest ability to forecast future TC events compared to the other environmental variables. Thus, when the performance of the E_{vws}, U_{mst} and $LLRV_{850}$ was compared, the $LLRV_{850}$ was the best, followed by the $E_{vws.}$.

The OLR predictors were characterized by negative exponential relationship between the predictors and TCs/TSs frequency suggesting that areas with low OLR (deep convection), favored TCs/TSs formation and development. The model output for the OLR predictor **Figure 9(b)** (blue curve) showed high level correlation ($r = 0.81$ at $p \leq 0.01$) between the fitted and the observed NM TCs as indicated by the level of goodness of fit (χ^2) (at $p = 0.87$). The model output was given by the Equation (11).

$$\ln\left(\mathrm{NMTCs}_{\mathrm{olr}}\right) = 39.47 - 0.04 * b_3 - 0.10 * b_{13} - 0.02 * a_{11} \tag{11}$$

where b_3 = November OLR at Southeastern Atlantic Ocean; b_{13} = SON OLR at Mediterranean Sea and a_{11} = July OLR at Southeastern Indian Ocean. This model designed from the environmental variable OLR model had the highest prediction skill of 43% and 61%, indicating that the model can foresee the future TCs by 61%.

3.6. The Performance of Dynamic, Thermodynamic and Combined Models for November to May Tropical Cyclones or Tropical Storms Season

The summary of the results of the performance of the three models (*i.e.* dynamic, thermodynamic and combined models) for the NM, TCs/TSs seasons are presented in **Table 2**. The results revealed that the SSTs predictors showed the least performance in predicting both TCs and TSs during the NM season. By contrast, the dynamic models had relatively higher performance with skill of 42% (MAE) and 61% (MSE). With these models the comparison between the observed and cross validated TCs/TSs frequency had a relatively stronger correlation factor ($r = 0.78$). However, the model cross validation sum of errors was relatively low (cv. ss = 0.03). For the NM TSs the model was characterized by the dynamic potential predictors which had high performance of 52.5% (MAE) and 76% (MSE) and lowest sum of cross validation errors of about 0.06.

Table 2. NM TCs/TSs model performance. Refer **Table A1** (in appendix) for model equation.

Type	NM TCs				NM TSs			
	r	RMSE	MAE_SS %	MSE_SS %	r	RMSE	MAE_SS %	MSE_SS %
Thermo dynamic	0.62	1.5	20	38	0.52	2.3	13.5	26
Dynamic	0.8	1.1	42	67	0.78	2.2	41.5	61
Combined model	0.8	1.1	39	64	0.87	1.6	52.5	76

Furthermore, the RMSE for the cross validated models ranged from 1.1 to 1.5 and 1.6 to 2.3 (Table 2) for the NM TCs and TSs, respectively. Moreover, the model analysis had revealed that the cross validated thermodynamic, dynamic and combined models during the NM season had Pseudo-R^2 ranged from 0.46 to 0.63 and 0.36 to 0.66 for the NM TCs and TS, respectively.

The inter annual variability of the cross-validated model outputs for the dynamic and combined models during NM TCs/TSs Figure 7(a) and Figure 7(b) showed strong correlations between the observed and the cross-validated model outputs for both the TCs and TSs showing best fitting of the curves. The results further indicated that both the observed and cross validated model out puts for dynamic and combined models were characterized by increasing TCs/TSs trends with higher TCs/TSs frequencies after 1994 than before 1994. By contrast, the thermodynamic model outputs for NM TCs/TSs showed poor correlation between the observed and the cross-validated model output, and the model was generally underestimated the forecasted TCs/TSs values in most years Figure 7(a) & Figure 7(b) (black curves).

3.7. The Performance of Dynamic, Thermodynamic and Combined Models for December to March Tropical Cyclone/Tropical Storms Season

The results on the performance of the three models in predicting the DJFM TCs/TSs are summarized in Table 5 As can be seen from Table 5 the two models (dynamic model and the combined model) had superior performance over the thermodynamic model for predicting DJFM TCs and TSs, with relatively higher correlation coefficients as well as model skills. The correlation (r) between the observed and cross validated model output results for the dynamic and combined model ranged between 0.78 to 0.86, while r for the thermodynamic model ranged between 0.62 and 0.73. The model skill performance for the dynamic and combined model based on MAE and MSE ranged from 37% - 49% (for MAE) and from 60% - 73% (for MSE). By contrast, the model skill performance for the thermodynamic model ranged from 21% - 31% (for MAE) and from 37% - 52% (for MSE).

The above presented results are consistent with the results presented in Figure 10 and Figure 11 which shows the inter-annual variability of the observed DJFM TCs/TSs frequency and the cross-validated DJFM TCs and TSs, where the curve fitting between the observed and the cross-validated model output values is slightly better for the dynamic and combined models than for the thermodynamic model. The results further revealed that the curve fitting for the thermodynamic model was generally worse for the DJFM TSs than for the DJFM TCs.

Furthermore, the RMSE for the cross validated DJFM TCs models ranged from 0.83 to 1.1 (Table 3), respectively. Moreover, the model analysis had revealed that the cross validated thermodynamic, dynamic and combined models during the NM season had Pseudo-R^2 ranged from 0.43 to 0.61 and 0.42 to 0.57 for the DJFM TCs and TS, respectively.

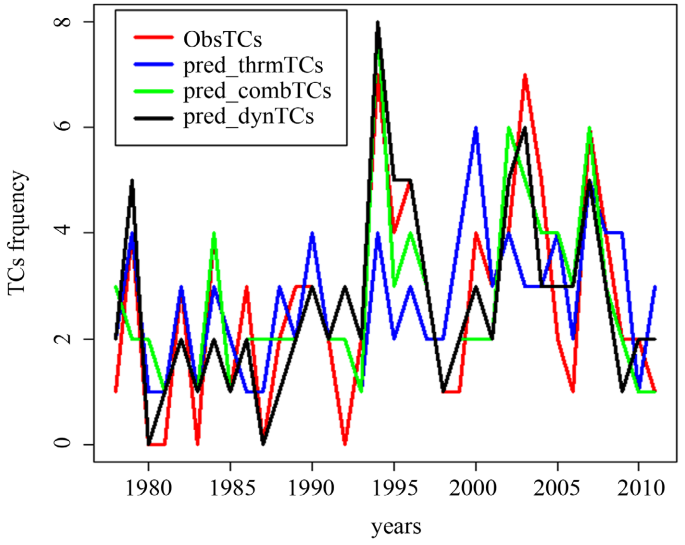

(a)

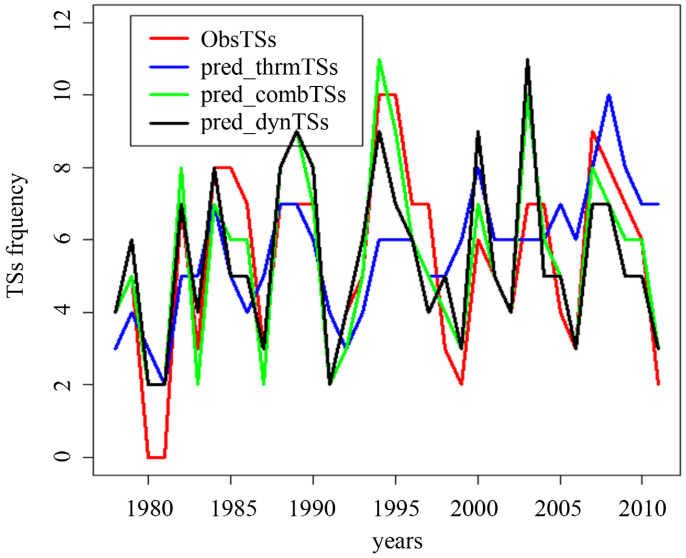

(b)

Figure 10. Cross validated models for NM TCs and TSs for dynamic; thermodynamic; and all parameter (combined) model (a) NM TCs models and (b) same like (a) but for NM TSs models..

Table 3. DJFM TCs/TSs model performance. Refer **Table A2** for model equations.

Type	DJFM TCs				DJFM TSs		
	r	RMSE	MAE_SS %	MSE_SS %	r	MAE_SS %	MSE_SS %
Thermo	0.73	1.1	31	52	0.62	21	37
dynamic	0.71		29	50			
Dynamic	0.86	0.83	46	73	0.78	37	60
Combined	0.84	0.85	47	69	0.85	49	72
model	0.84		47	70			

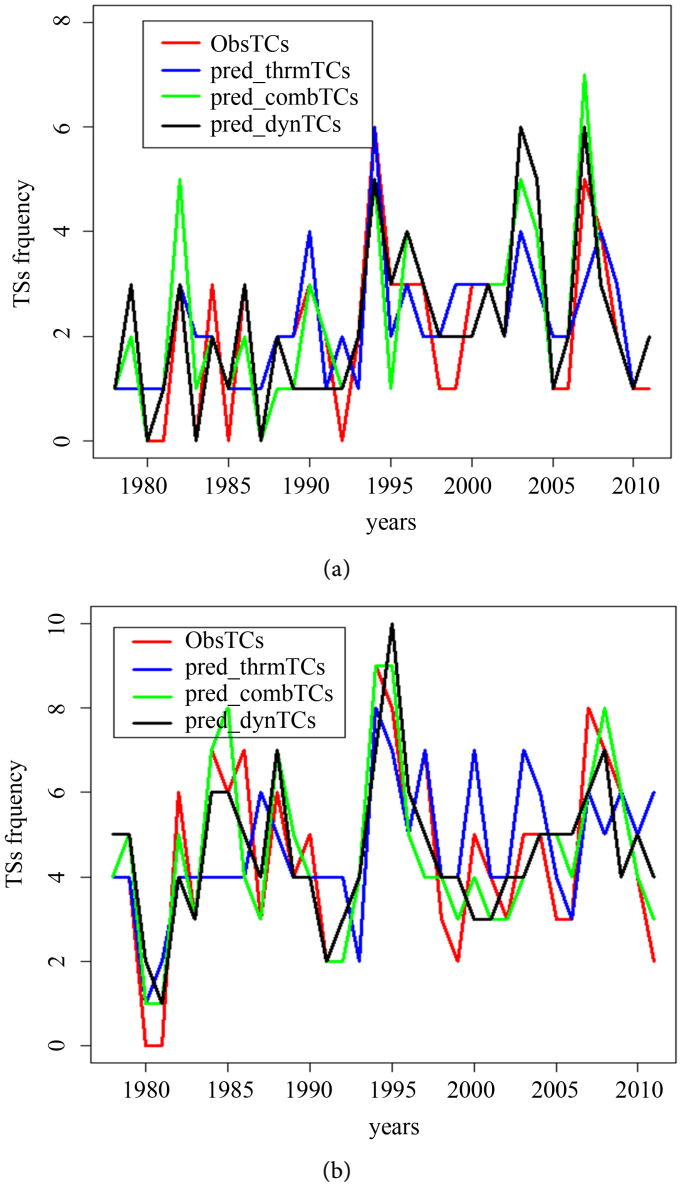

Figure 11. The cross validated DJFM TCs and TSs models for dynamic, thermodynamic and all parameter (combined) model (a) DJFM TCs and (b)same like (a) but for DJFM TSs models.

3.8. Verification Analysis of Cross Validated Seasonal Tropical Cyclone Models

Verification of the model performance using 2 × 2 contingency tables revealed that, during both NM and DJFM seasons, all models had the best value of zero for the false alarm ratio (*i.e.* proportion of the forecasted events that turn to being wrong (Table 4), whereas for bias (B) (*i.e.* comparison of average forecast and observation), all the three models showed that the forecasted and observed TCs frequencies were approximately equal Table 4 and Table 5. As for the proportion of percent correct (pc) and critical success's index (sci) the models had values ranging from 0.83 to 0.94, indicating that the models were doing very

Table 4. Analysis of the performance for the NM TCs and TSs models.

Model	NM TCs combined		NM TCs Thermodynamic		NM TCs dynamic		NM TSs combined		NM TSs Thermodynamic		NM TSs dynamic	
	OB	NOB	OB	NOB	OB	NOB	OB	NOB	OB	NOB	OB	NOB
F	29	0	29	0	29	0	32	0	32	0	32	0
NF	5	0	5	0	2	3	2	0	2	0	2	0
PC/CSI	0.85/0.85		0.85/0.85		0.94/0.93		0.94/0.94		0.94/0.94		0.94/0.94	
Bias	0.85		0.85		0.93		0.94		0.94		0.94	
FAR	0		0		0		0		0		0	

Note: OB = observed, NOB = not observed, F = forecasted, NF = Not forecasted, PC = percent correct, FAR = False alarm rate and CSI = critical successive index.

Table 5. Analysis of the performance for the DJFM TCs and TSs models.

Model	DJFM TCs combined		DJFM TCs Thermodynamic		DJFM TCs dynamic		DJFM TSs combined		DJFMTSs Thermodynamic		DJFM TSs dynamic	
	OB	NOB	OB	NOB	OB	NOB	OB	NOB	OB	NOB	OB	NOB
F	28	0	28	0	28	0	32	0	32	0	32	0
NF	2	4	6	0	3	3	2	0	2	0	2	0
PC/CSI	0.94/0.93		0.82/0.82		0.91/0.9		0.94/0.94		0.94/0.94		0.94/0.94	
Bias	0.93		0.82		0.9		0.94		0.94/0.94		0.94	
FAR	0		0		0		0		0		0	

good forecasts. However, in case of misses (*i.e.* observed TC/TS events but not forecasted), the combined and thermodynamic models for DJFM and NM TCs had highest missed of 6 and 5 as shown in Table 4 and Table 5. However, the presented results revealed that, all the three models had generally fewer miss in predicting TSs than in predicting TCs for both seasons (Table 4 and Table 5).

3.9. Verification Analysis of Cross Validated Seasonal Tropical Cyclone Models

Verification of the model performance using 2 × 2 contingency tables revealed that, during both NM and DJFM seasons, all models had the best value of zero for the false alarm ratio (*i.e.* proportion of the forecasted events that turn to being wrong (Table 4), whereas for bias (B) (*i.e.* comparison of average forecast and observation), all the three models showed that the forecasted and observed TCs frequencies were approximately equal Table 4 and Table 5. As for the proportion of percent correct (pc) and critical success's index (sci) the models had values ranging from 0.83 to 0.94, indicating that the models were doing very good forecasts. However, in case of misses (*i.e.* observed TC/TS events but not forecasted), the combined and thermodynamic models for DJFM and NM TCs

had highest missed of 6 and 5 as shown in **Table 4** and **Table 5**. However, the presented results revealed that, all the three models had generally fewer miss in predicting TSs than in predicting TCs for both seasons (**Table 4** and **Table 5**).

4. Discussions and Conclusion

4.1. Discussion

The SWIO Tropical cyclones and storms frequency for DJFM and NM seasons have been forecasted. In Tanzanian the DJFM season is characterized by a number of adverse impacts to the coastal society and their neighbor while the NM season, has its dynamics very much interrupted by March to May (MAM) rainfalls. Moreover, the former season had higher area averaged SSTs (>28˚C) and increasing trend of SSTs anomaly with higher spatial distribution of at least 0.4˚C at the Mozambican channel. These study findings are consistent with the studies of [11] [42] who indicted that low vertical wind shear and warm SST anomalies are conducive to more TCs activity. Furthermore, [42] found that over Mozambican channel majority of TCs are generated in January to February (JF), whereas [20] conclude that SSTs averaged over the region 8 - 22˚S and 50 - 70˚E can be used a predictor for TCs frequency (TCs days). Moreover, the observed high SST anomaly can be explained by the influence of northeast monsoon which causes a reversal of the Somali current, where coastal waters moves southwest and cooler air causes the surface water to cool and creates deep mixing. The east west variation of the Indian Ocean Dipole (IOD) could be another reason for this SST anomaly variation. The east west wind variation and zonal winds over 850 mb and 200 mb during the preseason (JJA) and during the onset of the season (SON) provides the changes in atmospheric circulation patterns to accommodate the TCs condition over SWIO, this argument is well approved by the presented results in **Figures 5-7** whereas the DJFM wind circulation (E_{vws}, U_{mst}) reveals the climatological wind circulation during the peak TCs season.

The presented results of the correlation between the Equatorial SOI and DJFM and NM TCs/TSs gave high correlations (at $p = 0.04$) between equatorial SOI, this can be linked with the climatology of the TCs in the SWIO where December to April have higher TCs and TSs records which are associated with the presence of higher SOI. This finding is consistent with that of [45] that higher SOI is associated with an increased likelihood of TCs in the early season. Moreover, the presented results of the Inter annual variability of TCs/TSs with U_{mst}, SST, equatorial SOI, and warm and cold episodes of ENSO among others, had provided the promising predictive skill where in most cases the peaks for the predictors and predictands were in phase following each other. The presented results based on the model performance for TCs and TSs during the NM season using single parameter models have shown good performed (**Table 1**), where for instance OLR model was the best by having high correlation between the observed and the fitted TCs ($r = 0.81$) and a prediction skill of 61%, indicating that, the deep convection over Southeastern Atlantic Ocean in the vicinity of Amazon Forests

during November, the July Equatorial Atlantic Ocean deep convection among others, have shown a good predictive skill in predicting the NM TCs. Though Indian Ocean SSTs have been proved to be a potential predictor for TC days prediction [4] as well as for TCs genesis and intensification [10] [41] but in this study, the area averaged SSTs over SWIO, have been out numbered in predicting the number (frequency) of TCs event. This less predictive skill of the SWIO area averaged SSTs could be contributed by the fact that, the correlation threshold which was set by this study in selecting the potential predictors was high. Besides, the SWIO SSTs potential predictors which had high correlations with TCs and TCs during DJFM and SON seasons were either had having low contribution in model coefficients (β value) or negative skill score. These arguments for SWIO SSTs to be out numbered in predicting the TCs and TSs frequency, could be consistent with [44] arguments that, the thermodynamic parameters play a more climatological role in tropical cyclogenesis, with their values varying little on a day-to-day basis.

The presented results of the correlation between the TCs frequencies and the September (–lead 2), October (–lead 1) northern Atlantic Ocean area averaged SSTs, and the April (lead 5) SOI have shown predictive value but with low skill (31% and 37% for single parameter and thermodynamic models of NM TCs). These presented results can be explained by northward shift of higher positive SST contour (28˚C during JJA to SON) over the northern Atlantic Ocean at the north western coast of Africa and North east south America (**Figure 4(b)**) and an increased SSTs due to warming of tropical Atlantic Ocean (which is much influenced by warm ENSO episodes). This tropical Atlantic Ocean warming, may course the Ocean evaporated moisture and heat to be transferred to Indian Ocean. Moreover, the increased SSTs over tropical Atlantic Ocean can also be explained by the positive polarity of the North Atlantic Oscillation (NAO) which is associated with the warming of the tropical Indian Ocean surface. Moreover, this finding and arguments (the ongoing discussion) are well supported by the findings of the studies by [45] [46] [47] [48].

The presented forecasting results of the DJFM TCs frequency using the thermodynamic prediction had improved the correlation coefficient between the observed and the cross validated TCs to be 0.73 using the September North Atlantic Ocean SSTs and October South Atlantic Ocean SSTs and to be 0.70 when the August Mediterranean Ocean SSTs were used instead of Southeastern Atlantic Ocean SSTs. Moreover, the model skill performance was increase from 37% with NM TCs to 52% with DJFM TCs. Based on the inter annual variability of the cross validated TCs, the presented results have shown that the model output was capturing most peaks of the observed TC frequencies with little under estimation of the forecasted TC frequencies.

The presented results have shown that, the Southeastern Atlantic Ocean SSTs had an impact to SWIO TC frequencies, this could be explained by the fact that Ocean currents may influence climate by transporting warm and cold waters to

other regions. For instance, South Atlantic Central Water and denser water masses are exported to the Indian Ocean through Retroflection (turns back on itself) of Agulhas current at Atlantic Ocean [49] [50] [51] [52]. Besides, the Subtropical Indian Ocean Dipole (SIOD) may have an influence to strength the relationship between the SWIO SSTs with TC frequency especially during DJFM where the SIOD is shifting further northward of the Mozambican Channel as well explained by [53] [54].

The presented results for the dynamic TC frequencies models during NM season have shown that, the model was dominated by vorticity from Eastern Namibia as well as from North eastern Madagascar during SON and November. These predictors resulted into a high degree of association (r = 0.8) between cross validated and observed TCs and higher prediction skill of 67%. On the other hand, the wind derived predictors have dominated the combined NM TCs model. For instance, the model was constructed using wind derived parameters of E_{vws} (*i.e.* September E_{vws} from Somali Sea), U_{mst} (November and July U_{mst} from Western Kenya and northwestern Atlantic Ocean), and North Atlantic Ocean SSTs. Moreover, the presence of U_{mst} predictors in the models could be explained by long track steering level 700 mb westerly and 200 mb easterly from North Atlantic Ocean and from Congo basin, as well supported by the study of [24], whereas September E_{vws} could be due to Oceanic low level (850 mb) northeasterly and upper level westerly.

For the DJFM TC frequencies, the dynamic model has been dominated by all wind derived parameter of U_{mst} (during SON over western Kenya), E_{vws} (during November over Northern Atlantic Ocean) and vorticity (during September over Northeastern South America). These potential dynamic predictors to DJFM TCs have resulted to a higher degree of association between the cross validated model output and observations (*i.e.* r = 0.86) with a prediction skill of 73%. The presented results of the all predicted and observed NM and DJFM TCs and TSs had shown to have high frequency during moderate El Nino conditions of 1994/1995, 1977/78, 1982/83, 1994/95, 2002/03, 2006/07 and 2009/2010, but did not capture the 1997/198 strong El Nino conditions which was mostly influenced by the reversal of the Indian ocean SST dipole mode from climatologically direction of west-east oscillation to east-west oscillation.

The environmental synoptic scales parameter derived from the winds (*i.e.* $U_{mst,}$ E_{vws}, and vorticity from different locations over land and Ocean) were having oscillation and division of high E_{vws} contours over southern latitudes which could be contributed the enhancement of the southward movement of genesis positions based on changes in vertical wind shear (*i.e.* E_{vws} is consistent with a warming-induced expansion due to general circulation over tropical atmosphere). This north south oscillation of high E_{vws} is well supported by [55] who found that, on average the latitude where TCs reach their peak strength has shifted farther north/south of the equator. This pole ward shift in latitude of maximum intensity could be a zonal average trend, where the pattern is strong in some basins but weaker/absent in others.

The presented results showed that, correlations between observed and cross validated TCs frequency, the skill scores, RMSE, MAE, and the pseudo R^2 were higher in dynamic and combined than in thermodynamic models, this was indicating that, the potential predictors for thermodynamic models was well explaining the variability of TCs frequency compared to potential predictors used in dynamic models. Moreover, in most cases the cross validated dynamic and combined models outputs and the observed were in phase and were having nearly the same patterns. Statistically the model verification performance using 2 × 2 square matrix and its contingency tables showed that all model types had scored higher values of percent correct item (pc) ranging from 0.85 to 0.94 with zero values of false alarm rate, whereas for the bias aspect the analysis revealed that, all the models had bias value of approximately equals to one, indicating that, the models were neither over forecasting no under forecasting. As for the aspect of misses, the results presented in Table 4 and Table 5 had shown that, TSs frequency models had few misses compared to TCs frequency models. For instance, out 34 TC events observed, 32 TCs events were correctly forecasted and observed and only two TCs events were not forecasted but were observed. The presented results for the dynamic models had shown that, out of 34 TCs events + 29 and 28 TCs events were correctly forecasted and observed, but 2 TCs events for during NM season and 3 TCs events during DJFM season were not forecasted but were observed, and 3 TC events were not forecasted and not observed at all.

4.2. Conclusions

1) Inter annual variability of SWIO TCs and TSs frequency during DJFM and NM seasons indirectly exhibits ENSO events and equatorial southern oscillation indices.

2) The variability of the Northern Atlantic Ocean SSTs has shown to impacts the TCs frequency over SWIO.

3) The penetration of warm SSTs northern Indian Ocean and linkage of retroflexed waters from the Agulhas which execute an equator ward meander of variable extent before proceeding eastward as well as positive (negative) mode of Indian Ocean Subtropical Dipole (IOSD) may have an influence to enhance the SWIO SSTs relation with DJFM and NM TCs/TSs frequency.

4) The wind derived environmental parameters of U_{mst}, E_{vws} and $LLRV_{850}$ accounts for 61% - 63% for the NM and DJFM TCs and 78% for TSs. This can be influenced by a westerly wind anomaly which extends across the tropical Atlantic and Africa at 700 mb, and 200 mb easterlies over the Atlantic Ocean that extend to the Indian Ocean.

5) The influence of wind derived parameters to SWIO TCs frequency may be contributed by Pacific-South Atlantic wave train (southern subtropical jet stream) which modulates SWIO wind shear.

5. Recommendations

More studies should be conducted to find more factors affecting the TSs and TSs

frequency and strength and their impacts to the seasonal rainfall of OND and MAM in SWIO basin and Tanzania in particular.

Acknowledgements

I would like to send my sincere appreciation to the ICPAC center at Nairobi for their willingness to direct me on how to download, handling and analysis of climate parameters. Moreover, I would like to acknowledge CCIAM project for providing me with the scholarship to pursue my PhD studies where this study is one of parts.

Conflicts of Interest

The authors declare no conflicts of interest regarding the publication of this paper.

References

[1] Jury, M.R., Pathack, B., Wang, B., Powell, M. and Raholijao, N. (1994) Distractive Cyclone Season South Western Indian Ocean. *South African Geographical Journal*, **75**, 53-59. https://doi.org/10.1080/03736245.1993.10586405

[2] Jury, M.R. (1993) A Preliminary Study of Climatological Associations and Characteristics of Tropical Cyclones in the S.W. Indian Ocean. *Meteorology and Atmospheric Physics*, **51**, 101-115. https://doi.org/10.1007/BF01080882

[3] Jury, R.M., Pathack, B. and Parcker, B. (1999) Climatic Determinants and Statistical Prediction of Tropical Cyclone Days in the Southwest Indian Ocean. *Journal of Climate*, **12**, 1738-1746. https://doi.org/10.1175/1520-0442(1999)012<1738:CDASPO>2.0.CO;2

[4] Jury, M.R. and Pathack, B. (1991) A Study of Climate and Weather Variability over the Tropical Southwest Indian Ocean. *Meteorology Atmospheric Physics*, **47**, 37-48. https://doi.org/10.1007/BF01025825

[5] Gallina, G.M. and Velden, C.S. (2002) Environmental Vertical Wind Shear and Tropical Cyclone Intensity Change Utilizing Satellite Derived Wind Information. 25*th Conference on Hurricanes and Tropical Meteorology*, San Diego, 28-29 April 2002, 172-173.

[6] Paterson, L.A., Hanstrum, B.N., Davidson, N.E. and Weber, H.C. (2005) Influence of Environmental Vertical Wind Shear on the Intensity of Hurricane-Strength Tropical Cyclones in the Australian Region. *Monthly Weather Review*, **133**, 3644-3660. https://doi.org/10.1175/MWR3041.1

[7] Chen, S.S., Knaff, J.A. and Marks, F.D. (2006) Effects of Vertical Wind Shear and Storm Motion on Tropical Cyclone Rainfall Asymmetries Deduced from TRMM. *Monthly Weather Review*, **134**, 3190-3208. https://doi.org/10.1175/MWR3245.1

[8] Gray, W.M. (1968) Global View of the Origin of Tropical Disturbances and Storms. *Monthly Weather Review*, **96**, 669-700. https://doi.org/10.1175/1520-0493(1968)096<0669:GVOTOO>2.0.CO;2

[9] Ho, C.-H., Kim, J.-H., Jeong, J.-H., Kim, H.-S. and Chen, D. (2006) Variation of Tropical Cyclone Activity in the South Indian Ocean: El Niño-Southern Oscillation and Madden-Julian Oscillation Effects. *Journal of Geophysical Research*, **111**, D22101. https://doi.org/10.1029/2006JD007289

[10] Arnold, A. (2012) An Overview and Brief History of Southern Hemisphere Tropical

Cyclones. http://www.csa.com/discoveryguides/discoveryguides-main.php

[11] Virtat, F., Anderson, D. and Stockdal, T. (2003) Seasonal Forecasting of Tropical Cyclone Landfall over Mozambique. *Journal of Climate*, **16**, 3932-3945. https://doi.org/10.1175/1520-0442(2003)016<3932:SFOTCL>2.0.CO;2

[12] Kai, K.H. (2018) Impacts of Southwestern Indian Ocean Tropical Cyclones and Storms on the Rainfall Pattern and Vegetation Productivity over Tanzania. PhD Thesis, Institute of Marine Sciences, University of Dar es Salaam, Dar es Salaam, 279 p.

[13] Kai, K.H., Ngwali, M.K. and Faki, M.M. (2021) Assessment of the Impacts of Tropical Cyclone Fantala to Tanzania Coastal Line: Case Study of Zanzibar. *Atmospheric and Climate Sciences*, **11**, 245-266. https://doi.org/10.4236/acs.2021.112015

[14] Kai, K.H., Osima, S.E., Ismail, M.H., Waniha, P. and Omar, H.A. (2021) Assessment of the Impacts of Tropical Cyclones Idai to the Western Coastal Area and Hinterlands of the South Western Indian Ocean. *Atmospheric and Climate Sciences*, **11**, 812-840. https://doi.org/10.4236/acs.2021.114047

[15] Mutemi, J.N. (2003) Climate Anomalies over Eastern Africa Associated with Various ENSO Evolution Phases, Ph.D. Thesis, University of Nairobi, Nairobi.

[16] Mahongo, S.B. and Shaghude, Y.W. (2014) Modeling the Dynamics of the Tanzanian Coastal Waters. *Journal of Oceanography and Marine Science*, **5**, 1-7. https://doi.org/10.5897/JOMS2013.0100

[17] Msemo, H.E., Finney, D.L. and Mbuya, S.I. (2022) Forgotten Accounts of Tropical Cyclones Making Landfall in Tanzania. *Weather*, **77**, 127-131. https://doi.org/10.1002/wea.3921

[18] Madden, R.A. and Julian, P.R. (1994) Observations of the 40 - 50 Days Tropical Oscillations: A Review. *Monthly Weather Review*, **122**, 814-835. https://doi.org/10.1175/1520-0493(1994)122<0814:OOTDTO>2.0.CO;2

[19] Landsea, C.W., Pielke Jr., R.A., Mestas-Nuñez, A.M. and Knaff, J.A. (1999) Atlantic Basin Hurricanes: Indices of Climatic Changes. *Climatic Change*, **42**, 89-129. https://doi.org/10.1023/A:1005416332322

[20] Mavume, A.F., Rydberg, L., Rouault, M. and Lutjeharms, J.R.E. (2006) Climatology and Landfall of Tropical Cyclones in the South West Indian Ocean. *Western Indian Ocean Journal of Marine Science*, **8**, 15-36. https://doi.org/10.4314/wiojms.v8i1.56672

[21] Vitart, F., Anderson, J.L. and Stern, W.F. (1999) Impact of Large-Scale Circulation on Tropical Storm Frequency, Intensity, and Location, Simulated by an Ensemble of GCM Integrations. *Journal of Climate*, **12**, 3237-3254. https://doi.org/10.1175/1520-0442(1999)012<3237:IOLSCO>2.0.CO;2

[22] Chang-Seng, D.S. and Jury, M.R. (2010) Tropical Cyclones in the SW Indian Ocean. Part 1: Inter-Annual Variability and Statistical Prediction. *Meteorology Atmospheric Physics*, **106**, 149-162. https://doi.org/10.1007/s00703-009-0055-2

[23] Chang-Seng, D.S. and Jury, M.R. (2010) Tropical Cyclones in the SW Indian Ocean. Part 2: Structure and Impacts at the Event Scale. *Meteorology Atmospheric Physics*, **106**, 163-178. https://doi.org/10.1007/s00703-010-0059-y

[24] Courtney, J. and Knaff, J.A. (2009) Adapting the Knaff and Zehr Wind-Pressure Relationship for Operational Use in Tropical Cyclone Warning Centers. *Australian Meteorological and Oceanographic Journal*, **58**, 167-179. https://doi.org/10.22499/2.5803.002

[25] Kalnay, E., *et al.* (1996) The NCEP/NCAR 40-Year Reanalysis Project. *Bulletin of*

American Meteorological Society, **77**, 437-472.
https://doi.org/10.1175/1520-0477(1996)077<0437:TNYRP>2.0.CO;2

[26] Trenberth, K.E. (1997) The Definition of El Nino. *Bulletin of the American Meteorological Society*, **78**, 2771-2777.
https://doi.org/10.1175/1520-0477(1997)078<2771:TDOENO>2.0.CO;2

[27] Liebmann, B. and Smith, C.A. (1996) Description of a Complete (Interpolated) Outgoing Longwave Radiation Dataset. *Bulletin of the American Meteorological Society*, **77**, 1275-1277.

[28] Smith, T.M., Reynolds, R.W., Peterson, T.C. and Lawrimore, J. (2008) Improvements to NOAA's Historical Merged Land-Ocean Surface Temperature Analysis (1880-2006). *Journal of Climate*, **21**, 2283-2296.
https://doi.org/10.1175/2007JCLI2100.1

[29] Chand, S.S. and Walsh, K.J.E. (2009) Tropical Cyclone Activity in the Fiji Region: Spatial Patterns and Relationship to Large-Scale Circulation. *Journal of Climate*, **22**, 3877-3893. https://doi.org/10.1175/2009JCLI2880.1

[30] Chand, S.S. and Walsh, K.J.E. (2010) A Bayesian Regression Approach to Seasonal Prediction of Troical Cyclones Affecting the Fiji Region. *Journal of Climate*, **23**, 3425-3445. https://doi.org/10.1175/2010JCLI3521.1

[31] Chan, J.C.L. (2006) Comment on "Changes in Tropical Cyclone Number, Duration, and Intensity in a Warming Environment". *Science*, **311**, 1713.
https://doi.org/10.1126/science.1121522

[32] Merrill, R.T. (1988) Environmental Influences on Hurricane Intensification. *Journal of Atmospheric Sciences*, **45**, 1678-1687.
https://doi.org/10.1175/1520-0469(1988)045<1678:EIOHI>2.0.CO;2

[33] Chan, J.C.L. and Gray, W.M. (1982) Tropical Cyclone Movement and Surrounding Flow Relationships. *Monthly Weather Review*, **110**, 1354-1374.
https://doi.org/10.1175/1520-0493(1982)110<1354:TCMASF>2.0.CO;2

[34] Elsner, J.B. and Schmertmann, C.P. (1993) Improving Extended Range Seasonal Prediction of Intense Atlantic Hurricane Activity. *Weather Forecasting*, **8**, 345-351.
https://doi.org/10.1175/1520-0434(1993)008<0345:IERSPO>2.0.CO;2

[35] Wilks, D.S. (1995) Statistical Methods in the Atmospheric Sciences. Academic Press, San Diego, CA, 467 p.

[36] McDonnell, K.A. and Holbrook, N.J. (2004) A Poisson Regression Model of Tropical Cyclogenesis for the Australian-Southwest Pacific Ocean Region. *Weather and Forecasting*, **19**, 440-455.
https://doi.org/10.1175/1520-0434(2004)019<0440:APRMOT>2.0.CO;2

[37] Noora, S. (2019) Estimating the Probability of Earthquake Occurrence and Return Period Using Generalized Linear Models. *Journal of Geoscience and Environment Protection*, **7**, 11-24. https://doi.org/10.4236/gep.2019.79002

[38] Kuleshov, Y., Qi, L., Fawcett, R. and Jones, D. (2008) On Tropical Cyclone Activity in the Southern Hemisphere: Trends and the ENSO Connection. *Geophysical Research Letters*, **35**, L14S08. https://doi.org/10.1029/2007GL032983

[39] Tuleya, R.E. and Kurihara, Y. (1981) A Numerical Study on the Effects of Environmental Flow on Tropical Storm Genesis. *Monthly Weather Review*, **109**, 2487-2506.
https://doi.org/10.1175/1520-0493(1981)109<2487:ANSOTE>2.0.CO;2

[40] Gray, W.M. (1975) Tropical Cyclone Genesis. Atmospheric Science Paper No. 234, Department of Atmospheric Science, Colorado State University, Fort Collins, CO.

[41] Gray, W.M. (1979) Hurricanes: Their Formation, Structure and Likely Role in the

Tropical Circulation. In: Shaw, D.B., Ed., *Meteorology over the Tropical Oceans*, Royal Meteorological Society, James Glaisher House, Grenville Place, Bracknell, 155-218.

[42] Roebber, P.J. and Bosart, L.F. (1996) The Complex Relationship between Forecast Skill and Forecast Value: A Real-World Analysis. *Weather and Forecasting*, **11**, 544-559. https://doi.org/10.1175/1520-0434(1996)011<0544:TCRBFS>2.0.CO;2

[43] McBride, J.L. (1981) Observational Analysis of Tropical Cyclone Formation. Part I: Basic Description of Data Sets. *Journal of Atmospheric Sciences*, **38**, 1117-1131. https://doi.org/10.1175/1520-0469(1981)038<1117:OAOTCF>2.0.CO;2

[44] Geerts, B. (1999) Trends in Atmospheric Science Journals: A Reader's Perspective. *Bulletin of the American Meteorological Society*, **80**, 639-651. https://doi.org/10.1175/1520-0477(1999)080<0639:TIASJA>2.0.CO;2

[45] Hoerling, M., Krishna, K.K. and Balaji, R. (2005) Advancing Dynamical Prediction of Indian Monsoon Rainfall. *Geophysical Research Letters*, **32**, L08704. https://doi.org/10.1029/2004GL021979

[46] Hoerling, M.P., Hurrell, J.W., Xu, T., Bates, G.T. and Phillips, A.S. (2004) Twentieth Century North Atlantic Climate Change. Part II: Understanding the Effect of Indian Ocean Warming. *Climate Dynamics*, **23**, 391-405. https://doi.org/10.1007/s00382-004-0433-x

[47] Bader, J. and Latif, M. (2003) The Impact of Decadal-Scale Indian Ocean SST Anomalies on Sahelian Rainfall and the North Atlantic Oscillation. *Geophysical Research Letters*, **30**, 2169. https://doi.org/10.1029/2003GL018426

[48] Li, S., Hoerling, M.P. and Peng, S. (2006) Coupled Ocean-Atmosphere Response to Indian Ocean Warmth. *Geophysical Research Letters*, **33**, L07713. https://doi.org/10.1029/2005GL025558

[49] Gründlingh, M.L. (1978) Drift of a Satellite-Tracked Buoy in the Southern Agulhas Current and Agulhas Return Current. *Deep Sea Research*, **25**, 1209-1224. https://doi.org/10.1016/0146-6291(78)90014-0

[50] Gordon, A.L., Weiss, R.F., Smethie, W.M. and Warner, M.J. (1992) Thermocline and Intermediate Water Communication between the South Atlantic and Indian Ocean. *Journal of Geophysical Research*, **97**, 7223-7240. https://doi.org/10.1029/92JC00485

[51] Lutjeharms, J.R.E., de Ruijter, W.P.M. and Peterson, R.G. (1992) Inter Basin Exchange and the Agulhas Retroflection; The Development of Some Oceanographic Concepts. *Deep Sea Research Part A. Oceanographic Research Papers*, **39**, 1791-1807. https://doi.org/10.1016/0198-0149(92)90029-S

[52] Lutjeharms, J.R.E. and Ansorger, I.J. (2001) The Agulhas Return Current. *Journal of Marine Systems*, **30**, 115-138. https://doi.org/10.1016/S0924-7963(01)00041-0

[53] Suzuki, R., Behera, S.K., Lizuka, S. and Yamagata, T. (2004) Indian Ocean Subtropical Dipole Simulated Using a Coupled General Circulation Model. *Journal of Geophysical Research*: *Oceans*, **109**, C09001. https://doi.org/10.1029/2003JC001974

[54] Ash, K.D. and Matyas, C.J. (2010) The Influence of ENSO and Subtropical Indian Ocean Dipole on Tropical Cyclone Trajectories in the Southwestern Indian Ocean. *International Journal of Climatology*, **32**, 41-56. https://doi.org/10.1002/joc.2249

[55] Kossin, J.P., Emanuel, K.A. and Vecchi, G.A. (2014) The Pole Wards Migration of the Location of Tropical Cyclone Maximum Intensity. *Nature*, **509**, 349-352. https://doi.org/10.1038/nature13278

Appendix

Table A1. The thermodynamic, dynamic and combined model equations for predicting the NM TCs and TSs frequency.

Type	Model equation for NM TCs
Thermo dynamic	$\ln(\text{NMTCs}_{\text{therm}}) = 21.35 + 0.41 * c + 0.68 * h + 0.26 * aprs$
Dynamic	$\ln(\text{NMTCs}_{\text{dyn}}) = 1.34 - 3.0 * 10^{5} * u_{19} - 1.9 * 10^{5} * u_{24} - 1.4 * 10^{5} * u_{26}$
Combined model	$\ln(\text{NMTCs}_{\text{comb}}) = -11.8 - 0.27 * h_{22} - 0.07 * d_{14} + 0.65 * h + 0.11 * h_{12}$
	Model equation for NM TSs
Thermo dynamic	$\ln(\text{NMTSs}_{\text{thrm}}) = -23 + 0.66 * cc + 0.50 * kai$
Dynamic	$\ln(\text{NMTSs}_{\text{dyn}}) = 3.6 - 8.6 * 10^{4} * uu_{15} - 1.4 * 10^{-01} * k_{11} - 6.3 * 10^{-02} * e_{10} - 4.4 * 10^{4} * uu_{45}$
Combined model	$\ln(\text{NMTSs}_{\text{com}}) = 5.1 - 9.6 * 10^{4} * uu_{15} - 1.8 * 10^{-01} * k_{11} - 8.1 * 10^{-02} * e_{10} - 4.4 * 10^{-02} * e_{20} - 3.3 * 10^{4} * uu_{45}$

Note that; c = September North Atlantic Ocean SST (0.51); h = October South West Atlantic Ocean SST (0.41); *aprs* = April ESOI (0.36); u_{19} = November Eastern Namibia LLRV850 (−0.45); u_{24} = SON Northeast Madagascar LLRV_{850} (−0.4); u_{26} = October Southern South Africa LLRV_{850} (−0.47); h_{22} = November Western Kenya U_{mst} (−0.45); d_{14} = September Somali Sea E_{vws} (−0.46); h_{12} = U_{mst} (−0.45); cc = June Equatorial AO SST (0.44); kai = September northwest AO SSTs (0.51); uu_5 = June Equatorial AO LLRV_{850} (−0.57); k_{11} = September South Western Indian Ocean U_{mst} (−0.43); uu_{45} = SON Eastern Namibia LLRV_{850} (−0.39); e_{20} = September South east South American E_{vws} (−0.39). Note the numbers within the brackets are their correlation with TCS or TSs during DJFM and NM TCs/TSs seasons.

Table A2. The thermodynamic, dynamic and combined model equations for predicting the DJFM TCs and TSs frequency.

Type	Models for DJFM TCs
Thermo dynamic	$\ln(\text{DJFMTCs}_{\text{thrm}}) = -28.5 + 0.76 * be + 0.76 * bk$, $\ln(\text{DJFMTCs}_{\text{thrm}}) = -22.6 + 0.74 * be + 0.31 * ax$
Dynamic	$\ln(\text{DJFMTCs}_{\text{dyn}}) = 1.88 - 1.4 \times 10^{-1} * k_{8} - 4.1 \times 10^{-1} * k_{26} - 9.2 \times 10^{-2} * e_{d20} - 2.0 \times 10^{5} * u_{8}$
Combined model	$\ln(\text{DJFMTCs}_{\text{com}}) = -10.4 + 0.5 * be - 0.1 * e_{20} - 0.1 * k_{8} - 0.4 * k_{26}$ $\ln(\text{DJFMTCs}_{\text{com}}) = -10.4 + 0.5 * be - 0.1 * e_{20} - 0.4 * k_{26}$
	Models for DJFM TSs
Thermo dynamic	$\ln(\text{DJFMTSs}_{\text{thrm}}) = 34.7 + 0.76 * c_{9} + 0.73 * c_{12} + 0.25 * b_{20}$

Continued

Dynamic	$\ln\left(\text{DJFMTSs}_{\text{dyn}}\right) = 2.02 - 5.57\times10^{-2} * g_{17} - 1.47\times10^{5} * vr_{12} - 8.64\times10^{4} * vr_{26}$
Combined model	$\ln\left(\text{DJFMTSs}_{\text{comb}}\right) = 3.68 - 4.77\times10^{-2} * g_{17} - 0.88e(-2) * g_{4} - 1.03\times10^{5} * vr_{26} - 1.33\times10^{5} * vr_{12}$

Note that; be = September North Atlantic Ocean SST (0.38); bk = October South East Atlantic Ocean SST (0.35); ce = SON South West Indian Ocean SSTS (0.41); ax = August Mediterranean Sea SST (0.41); k_8 = September South East South America U_{mst} (−0.47); k_{26} = SON Western Kenya U_{mst} (−0.47); e_{d20} = November North Atlantic Ocean E_{vws} (−0.45); u_8 = September North East South America $LLRV_{850}$ (−0.55); k_8 = September South East South America U_{mst} (−0.47). c_9 = September TUNIS OLR (−0.62); c_{12} = October North East Madagascar OLR (−0.36); b_{20} = August North Indian Ocean SSTs (0.4); g_1 = December South East Atlantic Ocean E_{vws} (−0.44); vr_{12} = August coastal Tanzania $LLRV_{850}$ (−0.53); vr_{26} = JJA north east south America $LLRV_{850}$ (−0.56); g_4 = July North West Africa E_{vws} (−0.55).